

Scotland's Rural College

Recent Progress in Carbon DotsBased Materials for Electrochemical Energy Storage Toward Environmental Sustainability

Siwal, Samarjeet Singh; Kaur, Harjot; Saini, Adesh K.; Thakur, Vijay Kumar

Published in:

Advanced Energy and Sustainability Research

DOI:

[10.1002/aesr.202200062](https://doi.org/10.1002/aesr.202200062)

Print publication: 01/09/2022

Document Version

Publisher's PDF, also known as Version of record

[Link to publication](#)

Citation for pulished version (APA):

Siwal, S. S., Kaur, H., Saini, A. K., & Thakur, V. K. (2022). Recent Progress in Carbon DotsBased Materials for Electrochemical Energy Storage Toward Environmental Sustainability. *Advanced Energy and Sustainability Research*, 3(9), [2200062]. <https://doi.org/10.1002/aesr.202200062>

General rights

Copyright and moral rights for the publications made accessible in the public portal are retained by the authors and/or other copyright owners and it is a condition of accessing publications that users recognise and abide by the legal requirements associated with these rights.

- Users may download and print one copy of any publication from the public portal for the purpose of private study or research.
- You may not further distribute the material or use it for any profit-making activity or commercial gain
- You may freely distribute the URL identifying the publication in the public portal ?

Take down policy

If you believe that this document breaches copyright please contact us providing details, and we will remove access to the work immediately and investigate your claim.

Recent Progress in Carbon Dots-Based Materials for Electrochemical Energy Storage Toward Environmental Sustainability

Samarjeet Singh Siwal,* Harjot Kaur, Adesh Kumar Saini, and Vijay Kumar Thakur*

Carbon dots (CDs), an emerging category of carbon nanomaterials, have bright destiny in a vast diversity of engineering areas due to their great variety in design, arrangement, and characteristics. Their possible implementations have recently traversed from electrochemical energy storage (EES), fluorescent probing, and catalysis, particularly as materials into the critical elements of the electrochemical system. Herein, the current investigation based upon the preface of CDs in batteries, supercapacitors, hydrogen/oxygen evolution reaction, oxygen reduction reaction, electromagnetic interference shielding, and solar-assisted energy generation used as electrode materials integrated with an active substance as an auxiliary mechanism is shown. Different aspects conferred upon selected illustrations outline the electrochemical activity, and eventually, current issues and future viewpoints are recollected toward the following optimization method of electrode substances. This review article is anticipated to demand broad attention within active CD materials and encourage the growth of high-performance EES systems.

1. Introduction

Recently, batteries, supercapacitors (SCs), and hydrogen/oxygen evolution reactions (HER/OER) electrolysis have grown within effective, dependable, and functional machineries toward electrochemical energy storage (EES) and converting electric power from sparkling energy origins, for example, solar, wind, geothermic, and waterfall.^[1] Although further progress within the electrode substances employed within these types of machinery is

still required, unique nanomaterials still require exploration to lower the price and acquire even better activity. In this respect, carbon-based nanomaterials (CNMs) with various forms and surface structures have been studied and broadly utilized in these EES types of machinery owing to their high quantity within nature, cost-effectiveness, better catalytic performance, high chemical/thermal durability's, enhanced specific exterior area, etc.^[2]

Carbon dots (CDs), 0D CNMs, including dimensions less than 10 nm, have been widespread due to their prominent quantum captivity and boundary consequences.^[3] CDs have been utilized to maintain the surface and conductive representatives for fabricating ingredients. These compounds have enhanced catalytic activity within applications, such as batteries, SCs, HER/OER, etc.^[4] Present studies show that CD-incorporated materials have


significant prospects as premium anode ingredients. For instance, Peng et al.^[5] briefed that CDs may be utilized upon electrode exteriors to fascinate additional cations and achieve high typical energy densities upon high temperature of CD hydrogel materials.

Further, Ji and his team synthesized MnO₂/CDs/GO electrode materials and recommended that the CDs work as a link to unite MnO₂ and graphene oxide (GO).^[6,7] In addition, they utilized CDs as an intercalator to design hybrid aerogels with

S. S. Siwal, H. Kaur
Department of Chemistry
M.M. Engineering College
Maharishi Markandeshwar (Deemed to be University)
Mullana-Ambala, Haryana 133207, India
E-mail: samarjeet6j1@mmumullana.org

A. K. Saini
Department of Biotechnology
Maharishi Markandeshwar (Deemed to be University)
Mullana-Ambala, Haryana 133207, India

V. K. Thakur
Biorefining and Advanced Materials Research Center
Scotland's Rural College (SRUC)
Kings Buildings, West Mains Road, Edinburgh EH9 3JG, UK
E-mail: vijay.thakur@sruc.ac.uk

 The ORCID identification number(s) for the author(s) of this article can be found under <https://doi.org/10.1002/aesr.202200062>.

© 2022 The Authors. Advanced Energy and Sustainability Research published by Wiley-VCH GmbH. This is an open access article under the terms of the Creative Commons Attribution License, which permits use, distribution and reproduction in any medium, provided the original work is properly cited.

DOI: 10.1002/aesr.202200062

V. K. Thakur
School of Engineering
University of Petroleum and Energy Studies (UPES)
Dehradun 248007, Uttarakhand, India

V. K. Thakur
Centre for Research and Development
Chandigarh University
Mohali 140413, Punjab, India

superior catalytical activity and advised that CDs would be employed as conductive agents. These investigations have revealed that CDs have significant assurance for implementation in electrochemistry.^[8]

CDs, a unique photoluminescent substance, have drawn significant concentrations because of their tunable photoluminescence (PL), remarkable electron transfer capabilities, economical, non-toxicity, and suitable hydrophilicity.^[9] Lately, Liu et al.^[10] suggested a known way to design low-ruthenium-content bimetallic materials for broad pH HER via carbon quantum dots. In addition, Lu and Wang^[11] focus on the current consequences of PL CDs and systematically examine the preparation of CDs. In particular, they highlight different transformation behaviors of fluorescence and afterglow emission.

The CDs may be instantly added to the preparation methods or developed utilizing facile (hydro/solvothermal, microwave-assisted preparation, elevated heat carbonization), electrophoretic deposition (EPD) and electrochemical deposit. The relationship among CDs' amalgamation, role, and effects is shown in a graphic chart illustrated in **Figure 1**.^[12]

Current investigations have suggested different methods for the large-range and economical preparation of CDs.^[12] For instance, Zhai et al.^[13] prepared CDs as new structure blocks for EES and electrocatalysis. Cheng et al.^[14] presented CDs' configuration and interface conversion for electrochemical energy utilization.

Here, this study will show the recent investigation based upon the preface of CDs within batteries, SCs, HER/OER, oxygen reduction reaction (ORR), electromagnetic interference (EMI) shielding, and solar-assisted energy generation used as electrode materials integrated with an active substance as an auxiliary mechanism. Different aspects conferred upon selected illustrations outline the electrochemical activity, and eventually, current hurdles and future outlooks are recollected toward the following development methods for electrode materials. This review article encourages the growth of high-performance EES systems and anticipated wide interest within active CD-based materials.

2. Carbon Dots in Different Dimensions

CDs, usually distinct as small carbon nanoparticles (CNPs) with numerous surface passivation arrangements, use and improve the inherent characteristics of the CNPs. Among different nano-scale carbon allotropes, fullerenes have intrinsically assumed the designation of CNMs on the 0D. Nevertheless, one can claim that fullerenes are, actually, stoichiometrically specified particles of not exclusive molecular arrangements but also different electronic networks and effects, basically distinct from CNMs in other sizes, such as carbon nanotubes (CNTs) and graphene nanosheets (GNSs) that evidently cannot be viewed as particles within any elasticity of the inventiveness.^[15] In contrast, small CNPs convey a critical structural characteristic with CNTs and GNSs, that is, structural and boundary faults (**Figure 2a**) is not feasible within fullerenes. Therefore, the NPs should deserve the label of nanorange carbon on the 0D.^[16] All the produced carbon outcomes, primarily the support system and the construction tools of the 1D N-, S-codoped carbon microrods, 2D N-, S-codoped carbon nanosheets (CNSs), and 3D N-, S-codoped carbon framework, are shown in **Figure 2b**. The construction of the 1D, 2D, and 3D CNMs may be separated into three phases. 1) The CDs were gathered and hidden upon the exterior of the supports. 2) The assembled CD sets obscured upon the template exteriors were restored to the related CNMs on high heat during pyrolysis. 3) The prototypes were released to get the matching CNMs with the congenital surfaces.^[17]

2.1. Structure

Owing to the vast assortment of publications associated with CDs, there is various and relatively confusing language within this field. CDs can be directed to carbon quantum dots (CQDs), carbon nanodots (CNDs), CNPs, etc. As there is no proof that quantum detention recreates a part within the PL tool toward these CDs, CQDs could not be correct, and CNP is a

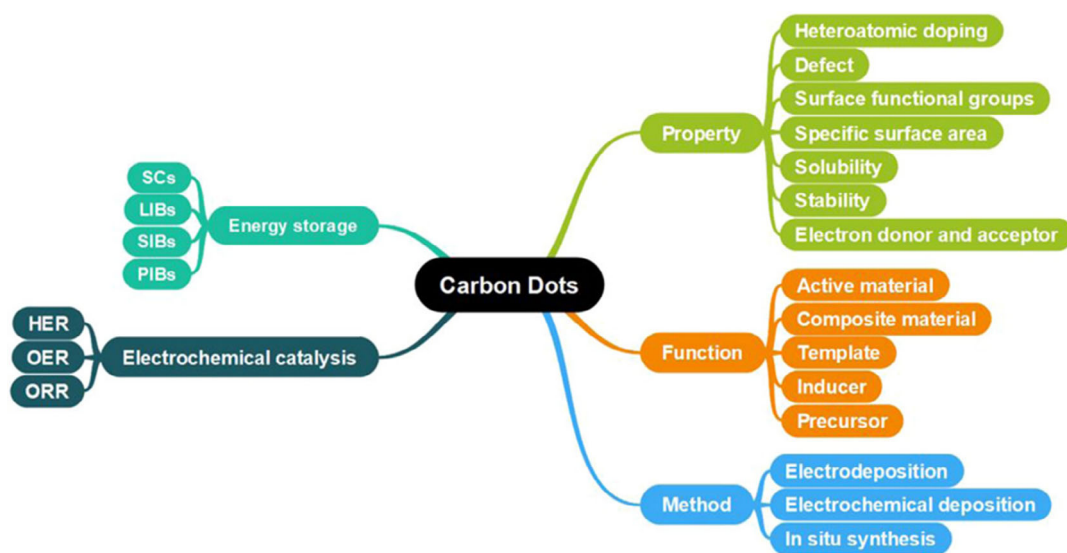


Figure 1. Graphic illustration of the association among the characteristic, function, and amalgamation approaches of CDs for EES and catalysis applications. Reprinted with permission under a Creative Commons CC BY 4.0 License.^[12] Copyright 2021, Wiley Online Library.

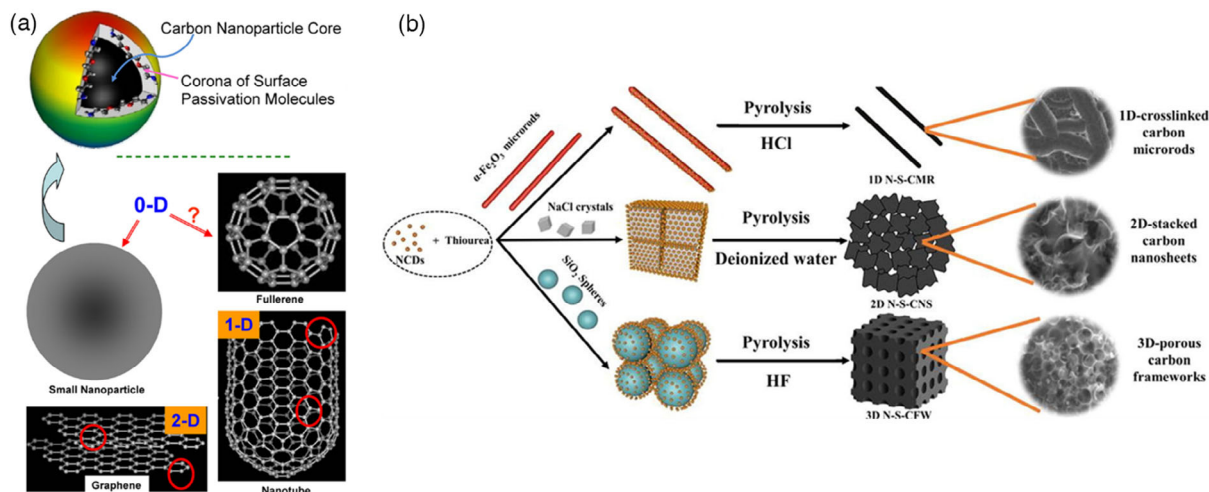


Figure 2. a) (Top) Cartoon description of a CD is typically a miniature CNP core with connected exterior passivation molecules into a structure identical to a smooth corona-like cover. (Bottom) CNMs within distinct dimensions, red rings show some fields toward possible structural and boundary defects. Reprinted with permission under a Creative Commons CC-BY License.^[16] Copyright 2020, American Chemical Society. b) Graphic preparation of 1D N-S-CMR, 2D N-S-CNS, and 3D N-S-CFW. Reprinted with permission.^[17] Copyright 2021, Elsevier Ltd.

broader term that does not supply much data concerning the particles. Likewise, to the problems with terminology, there are numerous hypothesized configurations for CDs examined upon a rare occurrence.^[18] Variable details for the structural arrangements that are barely unexpected as numerous reaction techniques and precursors are broadcast within the existing publications. One could predict divergent views, particularly for various top-down and bottom-up CDs. Further, a dispersal of dimensions is seen between all CDs, suggesting discrepancies, on the very minor, in the size of the arrangements seen in a sole CD trial. These concerns should be assessed while connecting data to CD design.

Mintz et al.^[19] intensely studied the configuration of CDs. This must be mentioned that there are outlying additional oxygen atoms upon the particle's exterior, but only specimen groups have been established within for clearness **Figure 3a**. Also, this is assumed that there is an s-triazine segment of the network based upon Fourier transform infrared spectroscopy (FTIR) and ¹³C nuclear magnetic resonance (NMR). The model was designed, as shown in **Figure 3b**. Regarding lattice classes, there should be two significant kinds: N₂-doped sp² carbon lattices and s-triazine networks that can unsystematically exist within the model. Only a mild oxidant exists toward Y-CDs reaction, and the process is just ultrasonication; therefore, these necessities would direct to the more kinetically prevented branched configuration. The model in **Figure 3c** was designed for viewing these components. It is considered that the diverged polymer may times on itself, relying upon the inflexibility of distinct branches of the polymer. This comparison will start with the three CDs' ultraviolet–visible (UV–vis) absorption effects (B-CDs, CNDs, and Y-CDs). There are distinctions even among identical peak places; nevertheless, absorption peaks of all 3-CDs lie within the 200–300 nm area (**Figure 3d**). The PL spectrum of individually CDs exhibited within **Figure 3e–g** indicates relatively disparate characteristics. However, the maximum excitation toward every species is 50 nm individually; the extremest lease

wavelength varies between 450 nm (CNDs), and 565 nm (Y-CDs), including B-CDs retaining, are lease utmost about 520 nm. This broad emission scope shows CDs' assortment and exhibits a remarkably diverse structural basis.

There are different characteristics and application areas of CNMs; within this study, we shortly concentrate upon the synthesis processes, properties, and energy storage applications of CDs. Hopefully, this study will offer practical understanding and facilitate a more profound quest for CDs.

2.2. Synthesis

Synthetic approaches for CDs may typically be categorized within two primary classes: top-down and bottom-up approaches. Top-down strategies direct the cutting of CNMs into CNPs; the techniques hold laser extirpation, arc liberation, electrochemical methods, and plasma processing. Bottom-up approaches contain the pyrolytic operation, template approach, reinforced synthetic process, microwave-supported process, chemical oxidation, inverse micelle process, etc. Some specific techniques are synthetic approaches, precursors, etc.^[20]

This process requires numerous steps in corrosion and exfoliation of cheap and readily obtainable carbon substances in extreme circumstances, essential oxidants, concentrated acids, and elevated temperatures. Instances of the top-down approach contain acidic exfoliation,^[21] electrochemical oxidation,^[22] metal-graphite embolism,^[23] hydrothermal combination,^[24] and robust physical ways, like arc release,^[25] electron ray lithography,^[26] laser excision,^[27] and nanolithography through reactive ion etching (RIE).^[28] However, it cannot precisely control the size diffusion and surface of the assembled particles with the top-down approach. It can utilize bottom-up approaches to prepare CDs from more small precursor molecules, such as the cyclodehydrogenation of polyphenylene^[29] and carbonization of distinct organic particles.^[30] Other bottom-up approaches comprise carbonization, pyrolysis, step-by-step chemical fusion, and solution

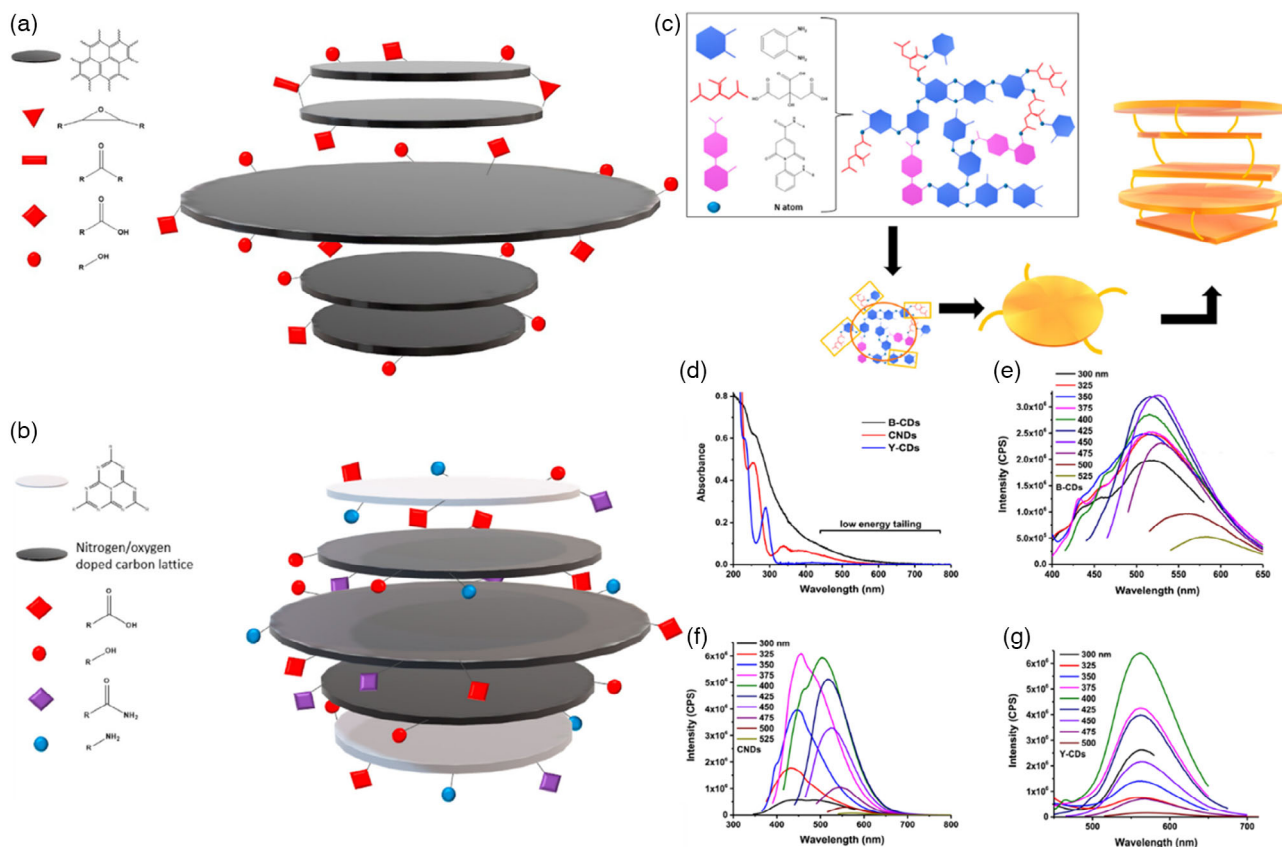


Figure 3. a) Hypothesized configuration sample of B-CDs. b) Hypothesized configuration sample of CNDs. c) Hypothesized configuration sample of Y-CDs. d) UV-vis spectrum and e) PL spectrum for B-CDs, f) CNDs, and g) Y-CDs. Reprinted with permission.^[19] Copyright 2021, Elsevier Ltd.

chemistry.^[31] However, a combination problematic during carbonization occurs.

3. Properties of Carbon Dots

CD-based materials have numerous engaging optical effects and superior biocompatibility.^[32] Notably, CDs exhibit steady performance within aqueous media with PL at visible wavelengths; the light discharged from CDs relies upon the excitation wavelength. These remarkable edges create CDs a good prospect compared with established organic pigments and semiconductor QDs that deliver possible use for visualization, photocatalysis, drug transfer investigation, and spectroscopic pursuits.^[33]

3.1. Structural and Compositional Properties

CDs, also comprehended as CNDs or CQDs, are quasispherical CNPs with particle dimensions under 10 nm and lattice spacing varying from 0.18 to 0.24 nm.^[34] They contain unstructured or nanocrystalline cores, including sp^2 groups.^[35] Few investigations have also documented diamond-similar networks constructed through carbon fractions having sp^3 hybridization.^[36] Qu et al.^[37] designed CDs via a single-step microwave preparation method containing sp^2 - and sp^3 -hybridized carbon bits. The dimensions and surface of CDs are illustrated utilizing

transmission electron microscopy (TEM) and atomic force microscopy (AFM) (Figure 4a,c). The TEM pictures show that the CD particles are spheroidal with an average dimension of around 2.6 ± 0.2 nm (Figure 4b). In addition, none of the lattice edges is marked within the related high-resolution TEM (HRTEM) picture (inset of Figure 4a), suggesting the unstructured character of the CDs. The AFM picture also sustains spherical surface, with intermediate sizes of around 1.8 ± 0.2 nm (Figure 4d).^[38]

FTIR or X-Ray photoelectron spectroscopy (XPS) may select functional surface clusters. Generally, moieties like C—O, C=O, and C—OH may typically present during the preparation procedure of prototypes and are present on the exterior of the prototype. In addition, distinct functional clusters may also be presented upon the exterior of CDs by choosing appropriate carbon predecessors or dopant precursors for the preparation operation. Dong et al.^[39] designed CQDs through low-heat pyrolysis of citric acid (CA) and radiated polyethyleneimine (BPEI). This one-step process checked the consequent CQDs with amino-abundant BPEI upon the exterior. CDs may also be functionalized postpreparation, usually involving numerous stages.

3.2. Optical Properties

Under the outstanding optical characteristics shown through fluorescent CDs, they have been harshly employed in various

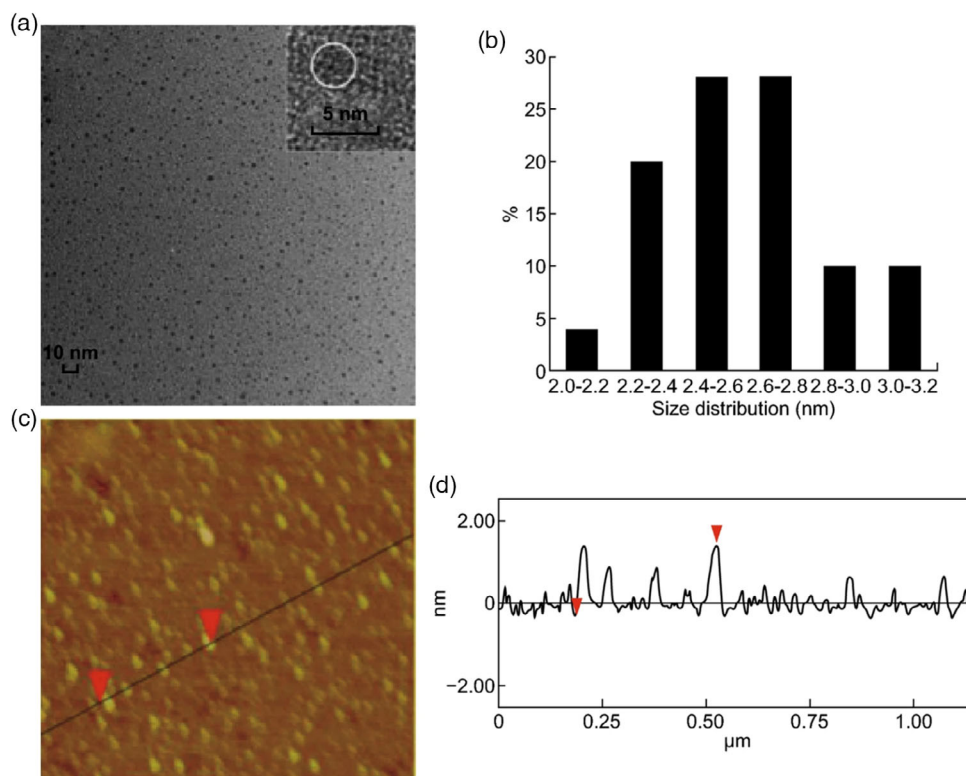


Figure 4. a) TEM pictures, b) size dispersal, and c, d) AFM picture and shape of CDs. Reprinted with permission.^[38] Copyright 2015, Elsevier Ltd.

healthcare implementations, particularly in biosensing, bioimaging, and treatment consequence. This is of significance to studying and comprehending CDs' optical effects to design a combination of CDs to help various bioapplications.

Generally, CDs effectively absorb light in the 230–340 nm short-wavelength regions with a tail lengthening within the visible parts. Due to changes in $\pi-\pi^*$ of C=C interactions of the core of carbon, the first absorption band of about 230–280 nm is discovered, and due to $n-\pi^*$ changes on the surface of C=O, the second band was obtained at nearly 300–340 nm.^[40] With the help of exterior passivation and doping of heteroatom, the absorption range may be modulated. For example, Das et al.^[41] designed three distinct kinds of incorporated CQDs, that is, incorporated with boron (BCQDs), coincorporated with boron and nitrogen (BNCQDs), and codoped with boron, nitrogen, and sulfur (BNSCQDs). The former two materials showed two bands while the latter showed three centered bands at 260, 320, and 440 nm. $\pi-\pi^*$ and $n-\pi^*$ evolutions of nonbonding orbitals and aromatic sp^2 domains are equal for the two more high-energy BNSCQDs, while because of the trapping of excited-state energy, the shifted band was obtained at 440 nm through specific surface conditions.

CDs' room-temperature phosphorescence (RTP) results are significant owing to their long lifetime. Two factors should be ideally taken into concern toward receiving RTP. The first involves suppressing nonradiative transitions by limiting process and vibration, while the second one desires to reduce the inter-system junction capability by augmenting the spin-orbit coupling via transition metals.^[42] On the other hand, RTP may

also be accomplished by CDs with crosslinked networks possessing non-conjugated classes.^[43] The construction of RTP within an aqueous solution is complex as phosphorescence quenching is generally followed in water because of the solvent-supported relaxation and liquefied oxygen.^[44,45]

Generally, the wavelength range of absorption peak of the CQDs is marked within 220–270 nm. As shown in Figure 5a, the absorption peak of electronic transitions from C—O or C=O bonds to π^* orbital lies within 280 ≈ 350 nm. The electron transitions of CQDs' exterior functional groups have an absorption peak wavelength in the range of 350–600 nm, representing that the surface chemical moieties can contribute to the absorption within the UV–vis region. Few investigations show that after the remediation with functional surface classes or by adjusting the sizes, the absorption peaks of CQDs redshift, as showcased in Figure 5b. Several notable CQDs display 600–800 nm long-wavelength absorption spectra originating from aromatic ring-containing structures, as shown in Figure 5c. Unlike earlier noted CDQs, the N-CQDs showed a robust excitonic absorption band owing to quantum-size consequences (Figure 5d).^[46]

4. Electrochemical Energy Storage Applications Toward Environmental Sustainability

4.1. Batteries

Carbon is one of the considerable significant elements within nature. CNMs, for example, CNTs and graphene (Gr), have

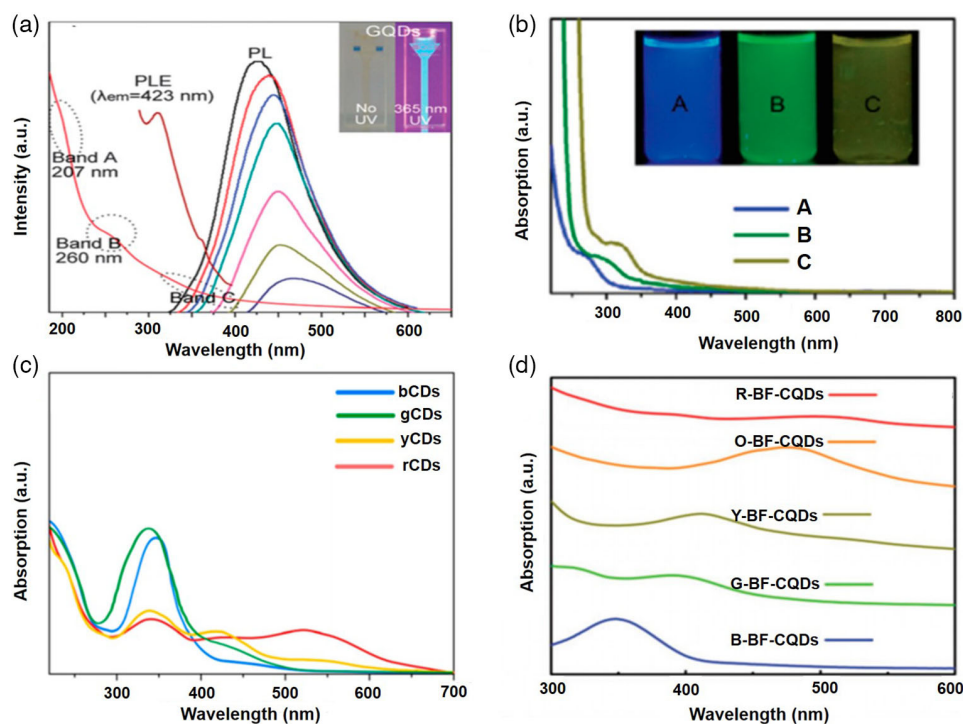


Figure 5. a) UV, PL spectra, and Photoluminescence excitation (PLE) spectra of CQDs assembled from graphite flakes. b) UV-vis spectrum of CDs under various reaction temperatures, correspondingly. c) Absorption spectrum toward long-wavelength emission CQDs. d) Absorption spectrum toward CQDs. Reprinted with permission.^[46] Copyright 2021, MDPI.

constantly been constituents of great respect to investigators and are broadly utilized in various areas. CDs are new types of CNMs, which stand out between the carbon allotropes. They are illustrated by their quantum dimensions, large external practical groups, consistent distribution, flexible configuration and arrangement, better biocompatibility, and PL effects. In 2004, a set of fluorescent NPs with a dimension of less than 18 nm was initially discovered by Xu et al.^[47] while filtering single-walled CNTs (SWCNTs) from arc fume cataphoresis. This unique kind of fluorescent CNM soon drew more concentration from investigators, and a type of synthesis strategy for CDs has been dug out.

In 2006, comparable CNPs with a width of ≈ 5 nm and improved fluorescence emission consequence were composed.^[27] They utilized argon (Ar) as a transport gas within laser excision of carbon targets with water vapor. Then the effects went via some processing, with exterior passivation and functionalization, and the CNPs with a unique character CD would be received eventually. Afterward, they performed a more extensive investigation upon nano-CDs. They discovered that surface passivation processing would remarkably enhance the quantum output of CDs, and the quantum output of CDs after cleavage and sanctification through column chromatography was elevated as 60%.^[48]

Although, these substances have their intrinsic imperfections. Inspired by the implementation of CDs in SCs, investigators initiated involving multifunctional CDs in battery designs in 2014,^[49] as illustrated in **Figure 6**. It was approved that electrode substances incorporated, including CDs, were practical approaches to crack multiple issues, for example, improving

electronic conductivity, enhancing ion communication, and regulating the dimensions and surface of the metal and metal oxides (MO_x). In addition, to electrode substances, the partitions and electrolytes also have a high effect on the catalytic activity of batteries. Astoundingly, CDs may also be utilized as transformers for partitions to accelerate ion communication and prevent dendrites' construction and electrolyte additives toward lithium-sulfur (Li-S) batteries to hinder the repeal and shuttle development of polysulfide-generated consistent Li deposit.

4.2. Supercapacitors

The most promising next-generation EES strategies, SCs, have drawn comprehensive investigation engagement owing to their high-energy density and storage capability, durable life, ecological cordiality, lightweight, and minor extent.^[50] SCs may typically be categorized into two types with various energy-storage tools: 1) electric double-layer capacitors (EDLCs) and 2) pseudocapacitors. In EDLCs, CNMs, in individual Gr and GO, are the select options because of their outstanding conductivity, elevated explicit exterior area, and extended cycle resilience.^[51] However, specific capacitances of EDLCs are determined owing to the non-Faradaic charge repository tool. In other words, pseudocapacitors exhibit 10–100 higher specific capacitances than the EDLCs due to the Faradaic charge storage tool's involvement with redox reaction taking a position within the bulk of active substances.^[52]

CDs are a unique family of CNPs below 10 nm that typically contain a nanocrystalline essence with central sp^2 -hybridized

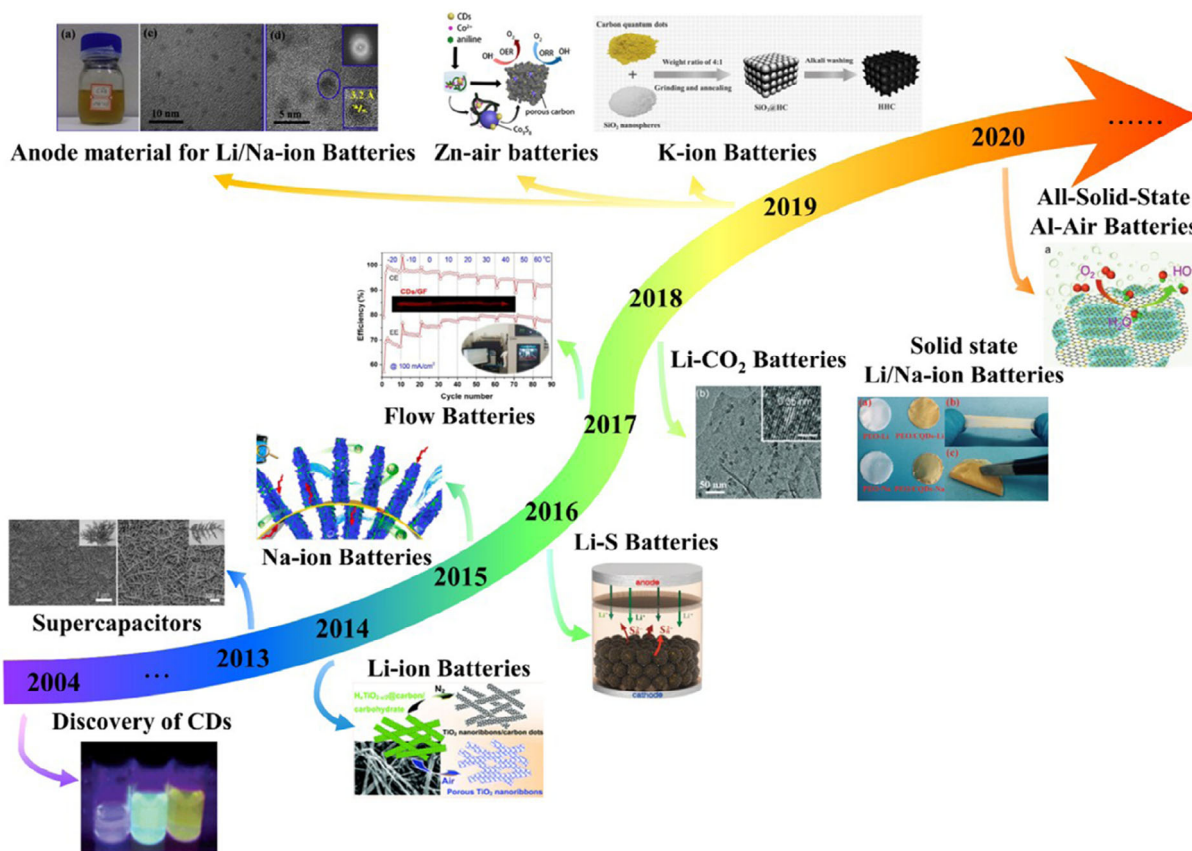


Figure 6. The consequence of implementations of CDs within developed batteries. Reprinted with permission.^[49] Copyright 2021, Elsevier Ltd.

carbon and an unshaped shell having large exterior operational groups.^[53] They show substantial PL with high quantum results and tunable bandgaps, therefore generally named CQDs, where GQDs are also incorporated. Multiple carbon-based substances (graphene, activated carbon, reduced graphene oxide, etc.) are used for SC utilization.^[54]

Zhang et al.^[55] prepared a ternary material of GO/CDs/PPy and utilized it as an active electrode composite toward SCs. **Figure 7a** shows that GO/CDs/PPy composite was incorporated through an improved in situ polymerization approach. **Figure 7b** illustrates the TEM photograph of CDs with a limited size dispersal histogram, confirming that as-prepared CDs are relatively consistent, having nearly 8.7 nm average sizes and having a variation of 1.4 nm. **Figure 7c** illustrates an expected TEM picture of the GO/CDs-2, where CDs particles may be noticed very obviously, adorning homogenously upon both flanks of GO layers. Also, an HRTEM picture (see the inset of **Figure 7c**) indicates the CDs with a lattice spacing of 0.215 nm into the crystalline body conforming the (100) characteristic of graphite. However, as for the GO/PPy representative, **Figure 7d** displays thick PPy layers that have been covered at equal edges of the GO sheet, and no CDs are located from its HRTEM picture (**Figure 7e**). On the other hand, black CDs may be noticed in the GO/CDs/PPy compound illustration from its HRTEM photograph, as illustrated in **Figure 7f**. Similarly, the ternary material GO/CDs/PPy hold the layered surface, likely owing to the asset

of the GO sheet (**Figure 7g**). As demonstrated in **Figure 7h**, galvanic charge–discharge (GCD) arcs were estimated utilizing 1 mol L⁻¹ aqueous LiCl media as an electrolyte in a three-electrode system. Similarly, GCD arcs of GO/CDs/PPy-2 at distinct current densities are offered within **Figure 7i**. Likewise, the catalyst’s cyclic voltammetry (CV) curves into a three-electrode design at a sweep rate of 10 mV s⁻¹ are exhibited in **Figure 7j**. A model EDLC displays a rectangular CV field, while the form transitions to a quadrilateral for EDLCs with resistive failures. In addition, CV arcs of GO/CDs/PPy-2 at different sweep rates of 5, 10, 20, 50, and 100 mV s⁻¹ (**Figure 7k**) contain established virtuous and steady capacitive manners under the circumstances of 1.0 V working potential. The catalysts were cycled 5000 runs on a current density (cd) of 10.0 A g⁻¹ to analyze their cycle strength (**Figure 7l**). The electrochemical impedance spectroscopy (EIS) study has been identified as one of the main approaches to investigate the essential manners of electrode substances for SCs. The resultant Nyquist plots (**Figure 7m**) contain a semicircle bend at the higher-frequency area and a linear bar at the lower-frequency site. Then the cadenced EIS graph was investigated by fitting the information by the equivalent circuit (the inset of **Figure 7f**).

As a result of the adsorption of CDs on the Gr’s surface, CD–Gr (CDG) hybrid media can be obtained. This adsorption primarily can take place via π - π relations (**Figure 8a**). The carbonization of ammonium citrate synthesized the CDs via easy dry

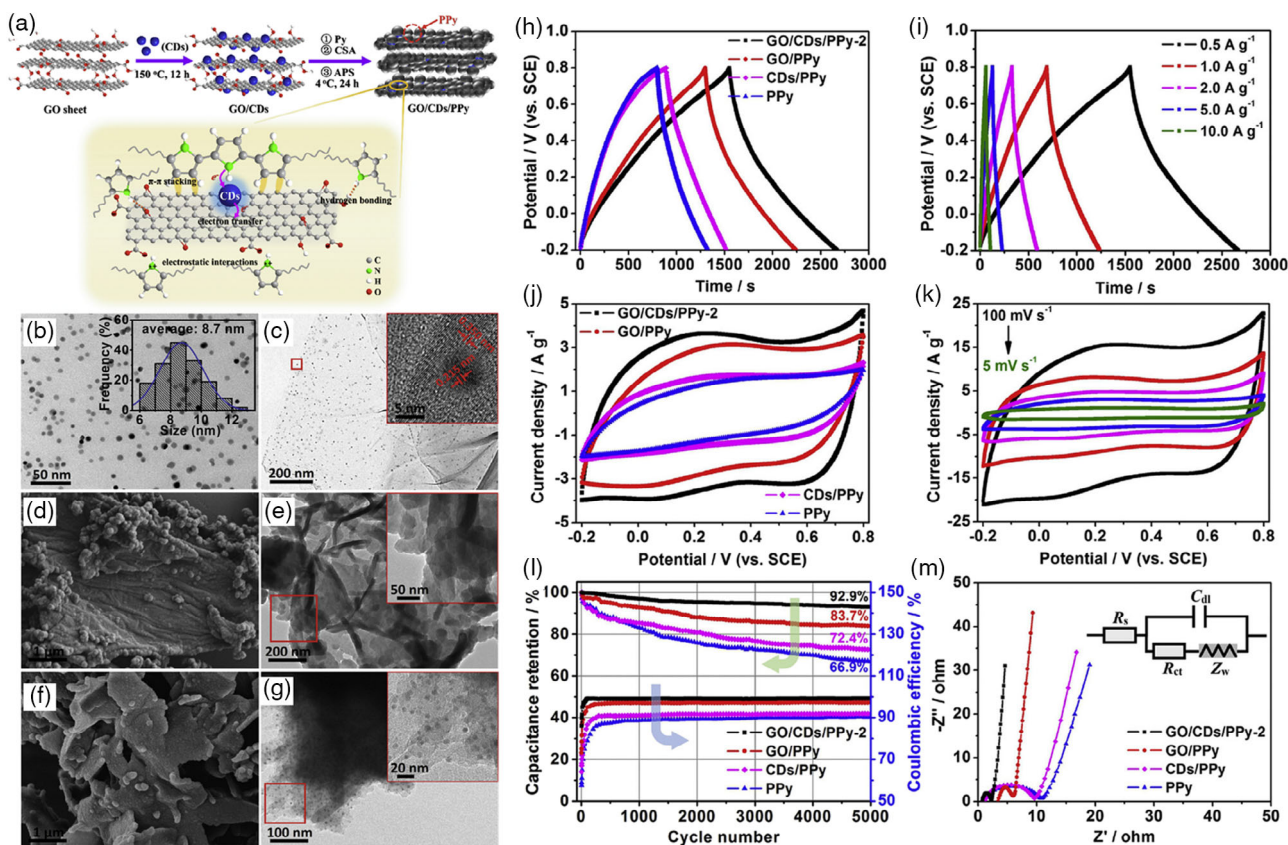


Figure 7. a) A graphic explanation of the preparation method of GO/CDs/PPy material. TEM photographs of b) CDs (inset: the lateral size dispersal) and c) GO/CDs-2 (inset: HRTEM photograph). SEM and TEM photographs of d,e) GO/PPy and f,g) GO/CDs/PPy-2 (inset: HRTEM photographs). The electrochemical activity of PPy, CDs/PPy, GO/PPy, and GO/CDs/PPy-2 materials in a three-electrode design: h) GCD arcs at a cd of 0.5 A g^{-1} ; i) GCD arcs of GO/CDs/PPy-2 at distinct current densities; j) CV arcs at a scan rate of 10 mV s^{-1} ; k) CV arcs of GO/CDs/PPy-2 recognized on different sweep rates; l) maintained specific capacitances and coulombic efficacy of anodes within 5000 GCD runs on a current density of 10.0 A g^{-1} ; m) Nyquist graphs within the frequency coverage from 100 mHz to 100 kHz (inset: the electrical equivalent circuit). Reprinted with permission.^[55] Copyright 2017, Elsevier Ltd.

heating (for 2 h at 180°C) technique. The as-prepared CDs, including 2–5 nm (Figure 8bb1), were readily liquefied within the water. The HRTEM photograph of CDs (the insert of Figure 8bb1) shows the graphitic interlayer arrangement of around 0.32 nm. The distribution of Gr (Figure 8cc1) within water is relatively low, owing to its positively aquaphobic character. CD-based materials possess polar functioning assemblies upon their exterior, which cause them to be soluble in water (Figure 8cc2), where the delocalized π -electrons of a carbon-enriched core having sp^2 character may reduce their connection with Gr via π - π relations. As displayed within Figure 8cc3, Gr comprises a satisfactorily spread and steady suspension within an aqueous CD media. Equal dispersion of CDs upon Gr is shown in the TEM pictures (inset of Figure 8bb2).

Furthermore, the promising stretchy electronics technology and planar energy apparatuses require better than planar SC appliances. So, they simulated a solid-state SC established upon manganese oxide CD graphene nanocomposites (MnO_x -CDGs) as the vigorous substance, *N*-methyl-2-pyrrolidone-polyvinylidene difluoride (NMP-PVDF) as dissolvable composite, and poly(vinylalcohol (H_3PO_4 /PVA) as electrolyte solution (Figure 8d) to enhance

elasticity and cyclic resilience. As may be noticed from CVs in Figure 8e, the solid-state SC maintained a 98.4% current value while the twisted slant was 90° , and it decreased to 81.2%, while the twisted slant was 135° . So, we may imagine that its catalytic activity was nearly not impacted till the twisting angle was capable of 90° , indicating that it may be utilized as a supple SC for relatively bending energy instrument implementations. Having a scope of sweep speed of $100\text{--}1600 \text{ mVs}^{-1}$, the solid-state SC (ss-SC) led to high current durability (Figure 8f). After 10 000 runs, MnO_x -CDGs achieved superior GCD cyclic resilience owing to the binder and gel media through a capacitive retaining value of 94.7% (Figure 8g), with cd around 1.2 A g^{-1} that was twofold more elevated compared with SC in the absence of NMP-PVDF binder and within $1 \text{ M Na}_2\text{SO}_4$ media. So, they combined two appliances into succession that delivered good capacitive characteristics within the voltage window between 0 and 2.0 V, as illustrated in Figure 8h. Figure 8i indicates the employment of an light-emitting diode (LED) driven by two appliances combined into succession.^[56]

Here, **Table 1** shows the applications and different parameters of CD-based materials in SCs.

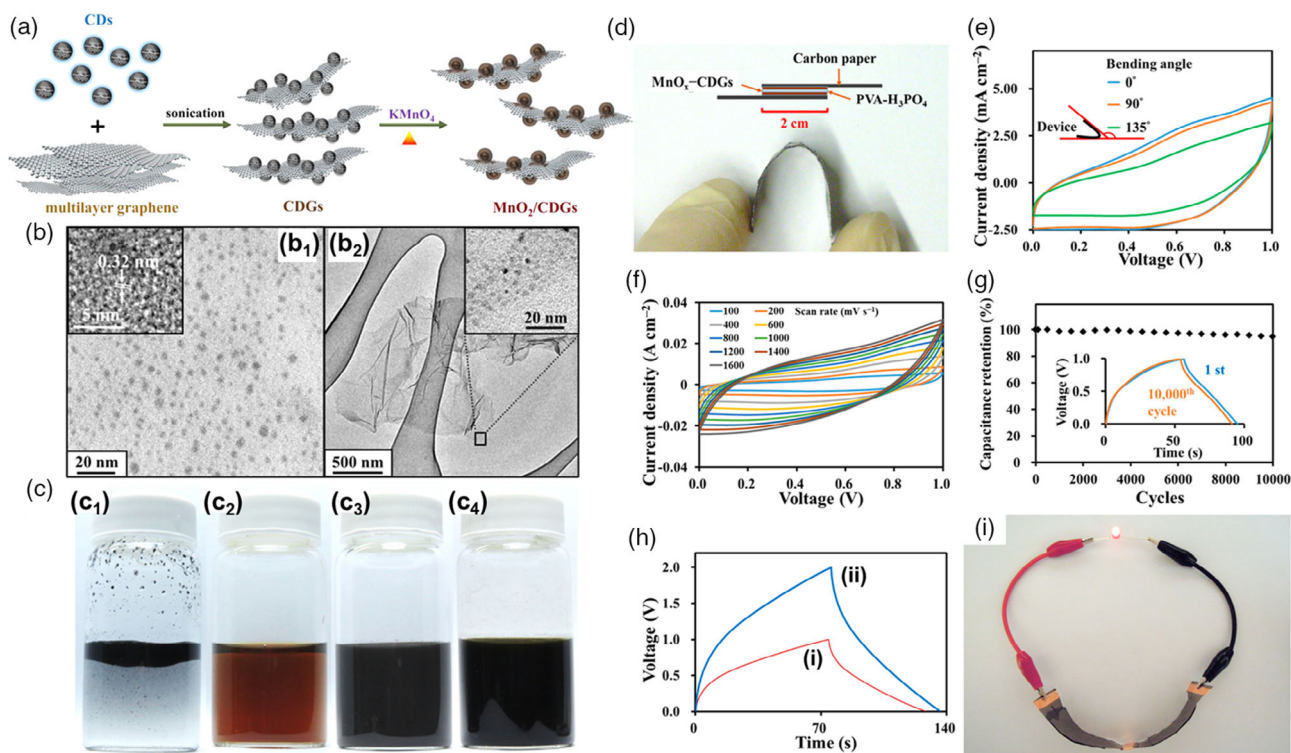


Figure 8. a) Graphic depiction of single-pot, lower-temperature preparation of MnO_x -CDGs composite utilizing CD as a sacrificial reductant. b) TEM pictures of b_1) CDs and b_2) CDG composite. (inset) HRTEM of b_1) CDs and b_2) MnO_x -CDGs. c) Vivid pictures of c_1) Gr, c_2) CDs, c_3) CDGs, and c_4) MnO_x -CDG distribution within water. d) Digital picture of the incorporated solid-state SC and its graphic presentation. e) CV cycles of MnO_x -CDG solid-state SC on the distinct twisted inclination on right angle, 0° , and 135° on a sweep speed of 100 mV s^{-1} . f) CVs of MnO_x -CDG ss-SC on special sweep rates. g) Durability examination of the MnO_x -CDG ss-SC of 10 000 GCD runs on a continuous cd at 1.2 A g^{-1} . (inset) GCD curves for the 1st and 10,000th runs. h) GCD arcs of i) one gadget and ii) two gadgets linked into succession, at a steady cd of about 1.0 A g^{-1} . i) LED-powered photos of 2-ss-SC linked within series. Reprinted with permission.^[56] Copyright 2016, American Chemical Society.

4.2.1. The Advantages of CD-Based Materials Compared with Other Types of Carbon-Materials in the Field of Electrochemical Energy Storage

CDs have become the formidable challenger for other carbon-based materials and other materials such as Pt- and Ir/Ru-based electrocatalysts due to chemical inertness, high electron mobility, cost-effectiveness, larger surface area, abundant surface defects, and active sites. The electrocatalytic performance of pure CD electrocatalysts can be enhanced via doping of heteroatoms like B, S, N, and P, which are utilized for electron-coupling interactions and to modulate electrical structures.^[44]

Presently CDs are primarily categorized as GQDs, CQDs, and carbonized polymer dots (CPDs) as per their various construction tools, micro-/nanostructures, and characteristics (Figure 9a). At the same time, we can build connections between them by adjusting the graphene film and carbonization degree. In comparison, the converted N and O co-doped CPDs within available porous 3D turbostratic graphene grids to manufacture SSCs (Figure 9b), ultimately acquiring quick charging paces with a relaxation period of 3.44 ms and energy density of 17.7 Wh kg^{-1} . It was a considerably more elevated comparison to the retail aluminium-based capacitor. Through developing hierarchical

porous carbon (HPC) substances from N-, P-, and O-codoped CPDs and polyacrylamide hydrogel (Figure 9c).

CDs can improve the storage capacity and electrocatalytic performance of nanomaterial when incorporated with other carbon materials, especially in SSCs. For ion intercalation/deintercalation, improving the capacitance of SSCs lattice strip with defects in CDs acts as layered structures.^[14] The incorporation of CDs provides more active sites for capacitance, and doped CDs provide additional faradaic capacitance, which improves the capacitance immensely. They can be used as electrode materials by incorporating them on different substrates along with their electrochemical performances. For instance, the GO/CDs/PPy composite was fabricated by Bi et al.^[55] under mild conditions via in situ polymerization of GO/CDs with pyrrole. The incorporated CDs surge the dielectric constant of the composite and facilitate the electron transfer through the active layer, which result in a high specific capacitance of 576 F g^{-1} at a current density of 0.5 A g^{-1} . It also exhibited outstanding cycling stability after 5000 cycles with 30.1 Wh kg^{-1} of energy density at a power density of 250 W kg^{-1} . Similarly, a micro-SSC based on GDs/graphene fiber was constructed by Chen et al.^[68] CD acts as a reinforcing nanofiller exhibiting superior mechanical strength of 109.93 MPa, which is three times larger as compared with bare graphene fiber. The as-synthesized material delivered

Table 1. Applications of CDs-based materials in SCs.

[CD]-based nanomaterials ^{a)}	Preparation method	Specific capacitance [F g ⁻¹]	Power density	Current density	Energy density	Capacitance retention	Technique used	Ref.
CQDs/polyaniline	Photoassisted electrodeposition route	738.3	0.3 mW cm ⁻²	1.0 mA cm ⁻²	169.2 mF cm ⁻²	78% after 1000 cycles	CV	[57]
Graphene quantum dot-doped polyaniline	–	1044	448.8 W kg	1 A g	117.45 Wh/kg	80.1 after 3000 cycles	GCD	[58]
CQDs/polypyrrole nanowires	Direct electrochemical method	306	224 W kg	0.5 A g	30.92 Wh kg ⁻¹	85.2 after 5000 cycles	CV	[59]
CQDs/MnO ₂ /graphene aerogel	One-step hydrothermal method	721	1 kW kg	1 A g	38.2 Wh kg ⁻¹	92.3% after 10 000 cycles	GCD	[6]
CDs/NiCo ₂ O ₄	One-step hydrothermal route	2168	216 W kg	1 A g	62 Wh kg ⁻¹	75% after 5000 cycles	GCD	[60]
CD/ Polyacrylamide	–	510	10 530 W kg	1 A g	90.1 Wh kg ⁻¹	96% after 5000 cycles	CV	[61]
TiO ₂ / sodium polyacrylate-derived CDs	One-step pyrolysis process	2200 mF cm ⁻²	635 μW/ cm ²	–	51.3 μWh cm ⁻²	91.43% over 5000 cycles	CV	[62]
Lignin-based activated carbon/ CDs	Chemical wet method	301	83 W kg	0.25	18 Wh kg ⁻¹	100% after 3000 cycles	GCD	[63]
Mn-Co LDH@CD	One-step hydrothermal route	2063	666 W kg	1 A g	79 Wh kg ⁻¹	74.1% after 3000 cycles	CV and GCD	[64]
CDs/ZnCo ₂ O ₄	Hydrothermal route	1937	425.3 W kg	1 A g	54.94 Wh kg ⁻¹	90% over 5000 cycles	CV	[65]
Co–NiS/NCDs	Two-step solvothermal route	2480	712 W kg	5 A g	71.6 Wh kg ⁻¹	78.3% after 12 000 cycles	GCD	[66]
NiCoHC/CDs	Hydrothermal method	1964.64	98.99 mW cm ⁻³	5 mA cm ⁻²	5.82 mWh cm ⁻³	76.1% after 3000 cycles	CV	[67]
Graphene hydrogel with lignin-based NCDs	Hydrothermal method	387	243 W kg	1 A g	25.6 Wh kg ⁻¹	92.3% after 5000 cycles	GCD	[68]
CDs/graphene fibers	Microfluidic-oriented strategy	60.1	–	0.1 mA cm ⁻²	67.37 μWh cm ⁻²	96% after 10 000 cycles	CV and GCD	[69]
NCDs/NiO/Co ₃ O ₄	Hydrothermal–calcination route	1775	800 W kg	1 A g	41.6 Wh kg ⁻¹	95.7 after 10 000 cycles	CV	[70]
NCDs/polyaniline	One-pot microwave and in situ oxidative polymerization	785	400 W kg	0.5 A g	49.9 Wh kg ⁻¹	70% after 2000 cycles	CV	[71]
NCDs/cobalt sulfide/rGO	Hydrothermal strategy	697	800 W kg	1 A g	36.6 Wh kg ⁻¹	85.9% after 10 000 cycles	CV	[72]
CDs/polypyrrole/graphene nameplates	Interfacial polymerization	173.81 mF cm ⁻²	–	1 mA cm ⁻²	–	96.3% over 2000 cycles	CV	[73]
Bi ₂ O ₃ / NCDs	Hydrothermal–calcination route	1046	770.9 W kg	1 A g	79.9 Wh kg ⁻¹	83.5% after 1500 cycles	CV and GCD	[74]
rGO@CD/ polyaniline	In situ polymerization and one-pot hydrothermal reduction	871.8	–	0.2 A g	–	72% over 10 000 cycles	CV and GCD	[75]

^{a)}LDH: Layered double hydroxides; Co–NiS/NCDs: nitrogen-doped carbon dots (NCDs)-decorated cobalt-doped nickel sulfide (Co–NiS) flower-like hierarchitectures.

long-term bending durability of 2000 cycles with large specific surface area of 435.1 m² g⁻¹ (almost double in comparison with bare graphene). A high capacitance of 607 mF cm² indicates its potential applications in flexible wearable electronics.

In addition to this, GQDs//GQDs material were synthesized by Liu^[24] and have outstanding power response, advanced rate capability up to 1000 V s⁻¹, and a high capacitance of 468.1 mF cm⁻² in an aqueous solution.

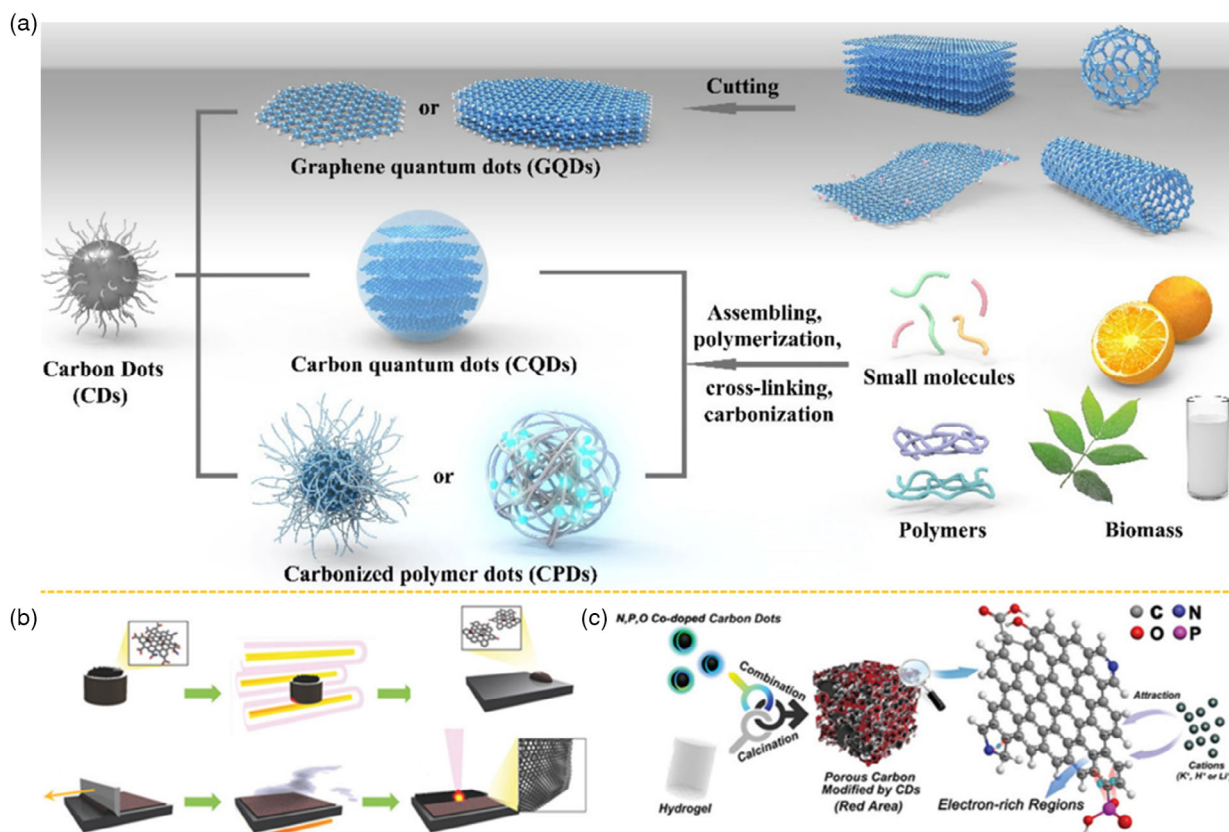


Figure 9. a) Category of CDs: such as GQDs, CQDs, and CPDs, and their main synthesis methods. Applications of CDs in SCs and rechargeable batteries. b) Representative of the transformation strategy. c) Porous carbon emanated from CPDs and polyacrylamide hydrogels. Reprinted with permission under a Creative Commons CC-BY License.^[44] Copyright 2020, American Chemical Society.

4.3. Hydrogen/Oxygen Evolution Reactions

The complete water oxidation comprises two half-cell reactions: OER and HER. Thermodynamical and dynamic investigations of these responses indicated lethargic reactions and required a higher voltage of 1.23 V to flow—a broad assortment of composites, for example, MO_x ,^[76] metal selenides,^[77] metal tellurides,^[78] metal sulfides,^[79] metal phosphides,^[80] metal–organic framework (MOF), etc. were used to overwhelm the energy borders of that response. This was found that Pt and oxides of Ir and Ru demonstrated more significant catalytic performance to overcome the energy barriers of HER and OER concurrently.^[81] However, the issue persisted, as these stimuli related to noble alloys were not economical. Their origins were insufficient, and they were considerably expensive between the other metallic element. These characteristics restricted their usage on a retail scale. Below these possibilities, an excursion to manufacture an Earth-abundant, ecological, vigorous, and profitable compound that can substitute these noble metal compounds and has the disposition to reach their electrochemical performance is on the form.

4.3.1. Hydrogen Evolution Reaction

Developing practical and affordable HER electrocatalysts for prospective renewable power systems is positively expected. CNMs

with exceptional edge locations, better chemical strength, elevated electrical performance, and synergetic consequences show tremendous potential. However, rare investigations have demonstrated the effectiveness of the CNMs upon catalytic performance. Toward renewable energy, H_2 is an illustrative energy porter, while for the accomplishment of good evolution of H_2 causes the creation of extremely functional electrocatalysts for HER acute.^[82]

The emission of carbon monoxide (CO) and carbon dioxide (CO_2) has evolved as the primary reason for environmental change, increasing global temperature. In addition, sulfur emission from fossil fuels directs to acid precipitation and sulfur mists. The surplus energy obtained by the periodic energy sources, for example, wind and sunlight, would be hydrogen kept by water splitting. Hydrogen gas created through steam reforming and coal gasification also leads to CO_2 release. Therefore, the electrocatalytic HER appears to be the weird approach toward collecting hydrogen.^[83]



The reaction appears on the catalyst's exterior, and the lower overpotential (η) and more elevated current density are achievable within the platinum (Pt) or its corresponding substances. However, Pt is very costly and not general smoothly. Typically, it lacks strength in a highly concentrated acidic environment

of polymer electrolyte fuel cells, which shows the reduction of H_2 in an enormous scale exhibition. Thus, studying an efficient and in situ way to simulate homogeneously spread metal NPs is definitely contained in a nanocarbon material through an economical path.

CQDs are promising nanomaterials that exhibit significant assurance toward bioimaging,^[84] optical sensing,^[85] catalysis^[86] and photovoltaic usages.^[87] CQDs with high strength, straightforward surface functionalization, and better electrical performance are appealing substances toward the configuration and incorporation of photoelectrocatalyst.^[88] The working assemblies (like, $-COOH$, $-NH_2$, $-OH$, $-CO$, and many more) upon the characters of the CQDs may correspond, including metal ions or semiconductors, having vacant *d*-orbitals for creating the reasonably steady CDQ–metal ions or semiconductors synchronization compound.^[89] The metal NPs are limited among the CQDs to create tremendous nanocrystals by steady networks that control the accumulation and development of the metal NPs throughout the reaction. Thus, CQDs can be an excellent transport for preparing metal HER materials.^[90]

Figure 10a illustrates the preparation of the compounds. Especially, CDs designed utilizing CA (CA; named CA-CDs), CA and ethylenediamine (EDA) (named CE-CDs), and CA and melamine (MA) (marked as CM-CDs) as feedstocks were

combined by a Mo and PA and after pyrolyzed for acquiring the definitive composites. Hexagonal structures of MoP are confirmed by the consequent X-ray diffraction (XRD) patterns (Figure 10b). Figure 10c indicates exact D- and G-bands on 1338 and 1590 cm^{-1} , correspondingly. The estimated I_D/I_G intensity proportion of MoP/0.5CM-CDs1100 of 1.13 shows multiple defects and disruptions within the Gr films. Figure 10d–f shows TEM photographs at various ranges of MoP/0.5CM-CDs1100, exhibiting the related carbon coatings that are conductive and advantageous toward reducing the core resistance of the amalgam composite.

Within 1.0 M KOH, a typical three-electrode technique was defined for the HER catalytic performances of the MoP/CDs materials. All voltages here direct to reversible hydrogen voltage. Figure 10h indicates that the related overpotential of 614 mV at a cd is about 10 mA cm^{-2} while no CDs were counted. The Tafel slant estimated by polarization arcs and EIS (Figure 10i,j) has the identical frequency as Figure 10h, indicating that the MoP/0.5CM-CDs1100 composite enriched with N content had the most promising HER activity. The strength of the MoP/0.5CM-CDs1100 composite was after that explained for 1000 CV runs (Figure 10k), while its η varied slightly on a cd of nearly 10 mA cm^{-2} . The HER catalytic activity of MoP/0.5CM-CDs800 to MoP/0.5CM-CDs1100 was chosen

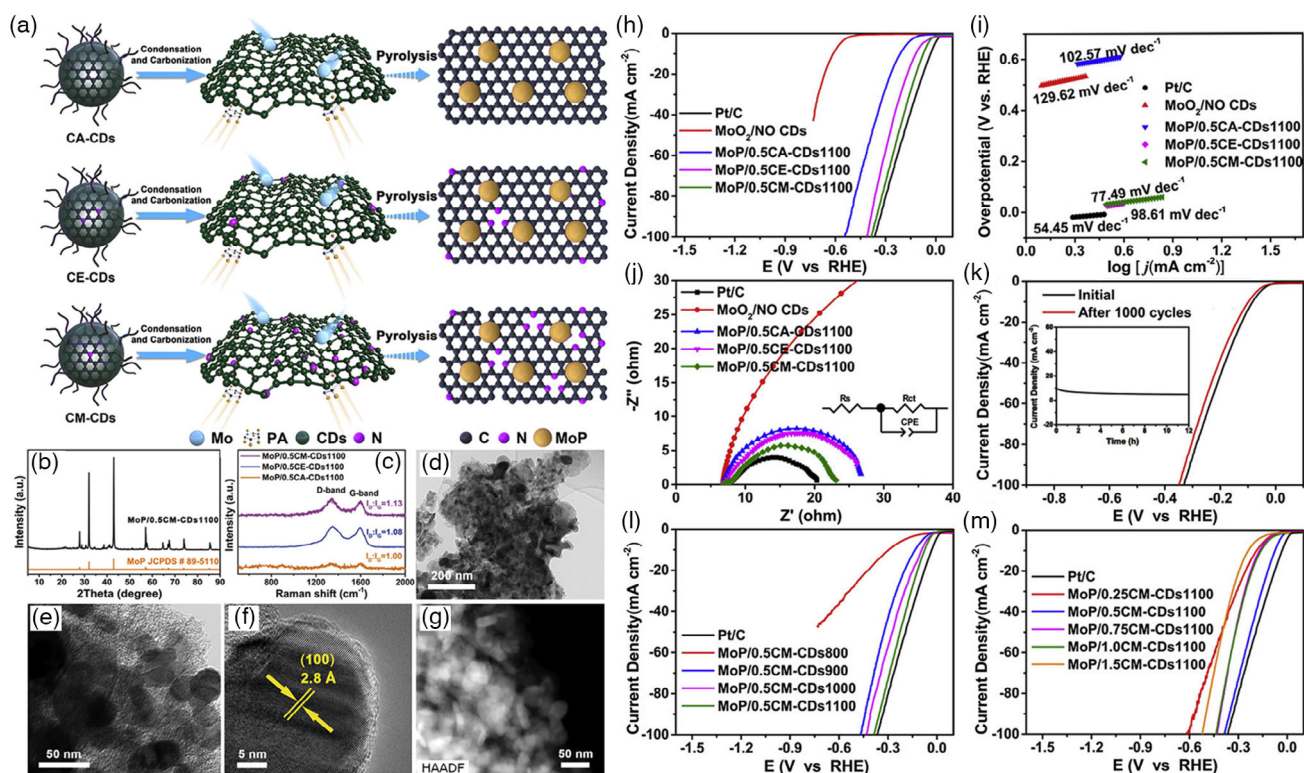


Figure 10. a) Graphic representation of the synthetic approach utilized toward the synthesis of the N-doped and defect-induced MoP/CD composite. b) XRD curves for MoP/0.5CM-CDs1100. c) Raman spectrum for different composites. d–f) TEM pictures of MoP/0.5CM-CDs1100 below distinct amplifications. g) High-angle annular dark-field picture. h) Polarization plots and i) equivalent Tafel slants of different materials at pH = 14. j) Nyquist plots for different catalysts as mentioned in figure. k) Sturdiness examination for MoP/0.5CM-CDs1100 within alkaline media initially and after 1000 runs. Inset: The current–time (*i*–*t*) arcs of MoP/0.5CM-CDs1100 on a persistent η for 12 h. l) Polarization arcs for the MoP/CM-CDs strengthened on distinct heat and Pt/C composite in 1M KOH media with a sweep rate of 5 mVs^{-1} . m) Polarization arcs of MoP/CM-CDs1100 synthesized through the addition of dissimilar CM-CDs proportions and profitable Pt/C into alkaline media. Reprinted with permission^[91] Copyright 2020, Elsevier Ltd.

utilizing a typical three-electrode configuration within an aqueous media 1.0 M KOH (Figure 10L). H₂ generation in water oxidation into a basic media was estimated (Figure 10m).^[91]

CDs are structurally mixed, inexpensive, readily incorporated (with N, B, S, and P), and nonhazardous. Their distinctive electron transfer effects and high explicit exterior area construct them as exceptional composites.^[92] They may sustain various surface-active groups (like, -NH₂, -OH, and -COOH) and host numerous favorable locations towards catalysis. Heteroatom-incorporated CDs may change the catalytically functional center's electronic configuration, facilitating adsorption of hydrogen intermediaries. The multicomponent nanostructures' relations could improve catalysis by reducing intermolecular electron transmission, essential for catalytic activity. Numerous earlier information on the hydrogen generation execution of RuP₂ amalgams have concentrated upon a one reaction procedure and have not assumed a sole composite toward H₂ generation through mutually the electrochemical HER of H₂O and the hydrolysis of ammonia borane.^[93]

4.3.2. Oxygen Evolution Reaction

Demand to follow the origins of energy fascinates humankind to see a renewable source with tremendous reservoirs during its carriage with no dangerous consequence to humanity. These days, the energy-lacking globe is desiring an electrocatalyst with a facile and straightforward preparation process with outstanding

catalytic activity and outstandingly sustained strength toward the positively sluggish OER.^[94]

The OER is a favorable energy transformation strategy examined in the current years. Nevertheless, due to the elevated η and lethargic kinetics of the OER, an effective catalyst is essential toward lowering the η and accelerating the reaction. This description informs cobalt phosphide (CoP)/CD materials as a composite toward the OER.^[95] CDs have produced tremendous concentration as fluorescent searches for detecting heavy metals because of their exceptional characteristics, like cost effectiveness, easy operating ways, useful photostability, simple functionalization, low toxicity, adequate water solubility, and superior conductivity.^[96] These remarkable characteristics have evolved widespread into bioimaging, optoelectronic appliances, photocatalysis, sensors, and electrocatalytic water splitting (OER).^[97] Nowadays, different precursors and techniques have been used to manufacture CDs. However, most outcomes show short emission beneath UV-vis radiation that is not conducive to functional usage.^[98]

OER composites based upon transition metal oxides (TMO_x), particularly NiO, have improved consideration owing to their extensive resources, low loss, and similar catalytic performance.^[99] NiO, a standard semiconductor with the expansive bandgap energy of 3.6–4.0 eV, maintains superior redox reversibility, enormous exterior areas, and better performance and has been broadly investigated as a reason for an excellent electrochemical composite toward OER.^[100]

For instance, **Figure 11a** shows the incorporation of polarized-SO₃-CDs/NiFe LDH (P-SO₃-CDs/NiFe LDH) composite anode

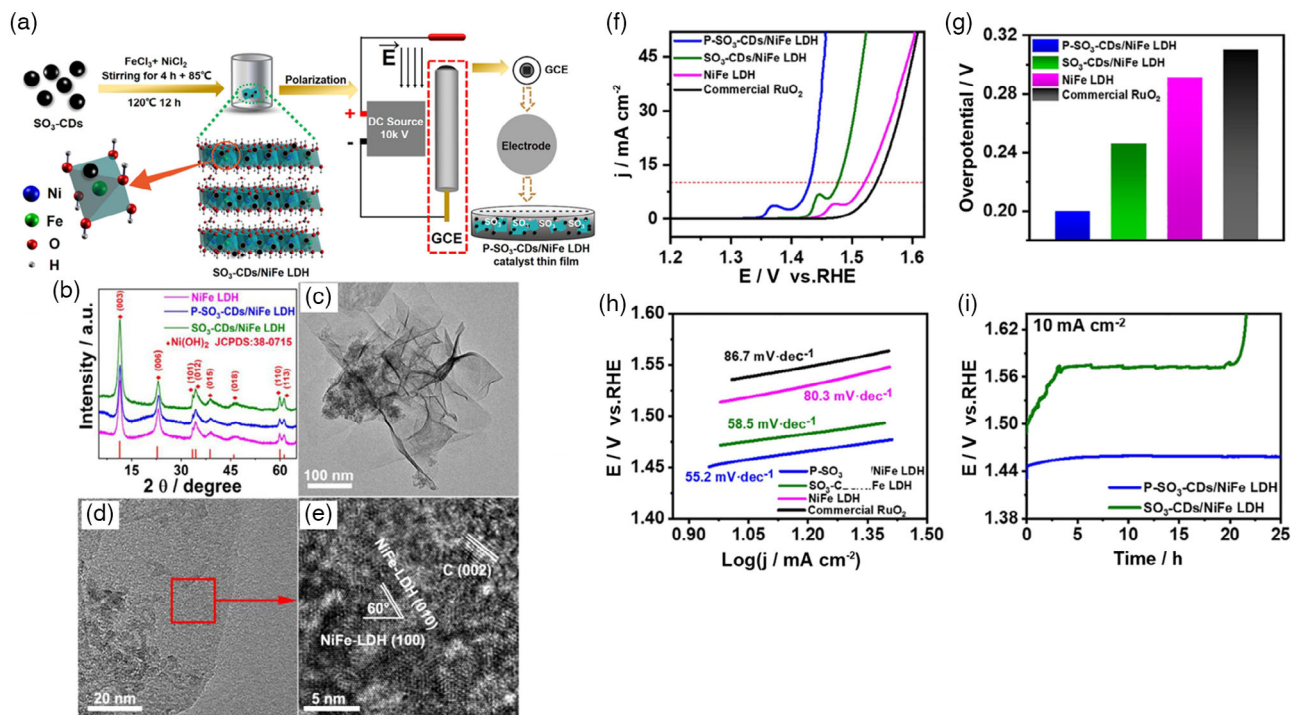


Figure 11. a) Graphic representation of working electrode incorporation procedure. Description of NiFe LDH materials. b) XRD patterns of the synthesized materials. c, d) TEM pictures and e) HRTEM picture of SO₃-CDs/NiFe LDH. The catalytic activity of NiFe LDH-based OER composites: f) IR-remended polarization arcs of different composites within alkaline media. g) η of the synthesized OER composites. h) Tafel slopes of the synthesized OER composites. i) Chronopotentiometry arcs of synthesized materials on 10 mA cm⁻², correspondingly. Reprinted with permission.^[101] Copyright 2021, Elsevier Ltd.

electrodes. Figure 11b illustrates the XRD patterns for $P\text{-SO}_3\text{-CDs/NiFe LDH}$, $\text{SO}_3\text{-CDs/NiFe LDH}$, and NiFe LDH. The surface, dimensions, and configuration of the $\text{SO}_3\text{-CDs/NiFe LDH}$ were also described via TEM, as depicted in Figure 11c–e, indicating sized nanofilms of 50–200 nm. This is nearly translucent beneath the e^- -ray owing to its very thin character. Three reference specimens were also experimented under identical circumstances for comparison. Figure 11f shows the IR-corrected linear sweep voltammetry (LSV) graphs of OER of synthesized materials. As demonstrated in Figure 11f,g, in $P\text{-SO}_3\text{-CDs/NiFe}$, better OER activity was shown by LDH, including η of 200 mV on a cd of 10 mA cm^{-2} , that is, 46 mV less than $\text{SO}_3\text{-CDs/NiFe LDH}$ (246 mV), 91 mV less as compared with NiFe LDH (291 mV) and 110 mV less as compared with the retail RuO_2 (310 mV). As demonstrated in Figure 11h, Tafel plot of $P\text{-SO}_3\text{-CDs/NiFe LDH}$ was obtained at 55.5 mV dec^{-1} and showed the most rapid kinetics, which is smaller as compared with $\text{SO}_3\text{-CDs/NiFe LDH}$ (58.5 mV dec^{-1}), NiFe LDH (80.3 mV dec^{-1}), and the retail RuO_2 (86.7 mV dec^{-1}), correspondingly. Furthermore, $P\text{-SO}_3\text{-CDs/NiFe LDH}$ showed the uppermost performance of the composite estimated and achieved better electrochemical durability. Figure 11i indicates that the stability of the synthesized compound was estimated on the cd of 10 mA cm^{-1} . Likewise, after the count of sulfonated CDs around Fe atoms of NiFe LDH, there are also three middle forms within the OER method. The better catalytic performance was primarily ascribable toward NiFe LDH, while the accumulation of $\text{SO}_3\text{-CDs}$ improved OER performance.^[101]

4.3.3. Oxygen Reduction Reaction

The need for competitive options for noble platinum as a positively active ORR material has improved because the retail implementations of Pt-based composites are restricted via their high price, CO inactivation, and insufficient stability.^[102] Different methods have been investigated to substitute retail Pt-based composites with metal-free CNMs. Metal-free-based composites retain necessary characteristics, for example, better electrical performance, high exterior area, and moderately good strength.^[103] Within the carbon material family, CQDs, or CDs, a new type of 0D nanocarbon with dimensions under 10 nm exhibited better solubility, low cytotoxicity, excellent quality compatibility, and facile preparation functionalized by exterior passivation. CDs have positively inferior oxygen-possessed moieties dispersed unsystematically on the basal plane and border areas.^[104]

Current research indicates that N-doped CNMs appear to be an exemplary process for promoting ORR. For example, Qu et al.^[105] prepared N-doped GQDs (N-GQDs) through CV cycles. The as-synthesized N-GQDs with an N/C atomic proportion of $\approx 4.3\%$ showed outstanding electrocatalytic capability toward ORR. Lee et al.^[106] showed vigorous hydrothermal preparation of N-doped CDs (N-CDs) by the unripe peach toward fluorescent bioimaging and catalytic ORR. Likewise, N-doped Gr (NG) was prepared via distinct processes such as chemical vapor deposition,^[107] plasma processing,^[108] and thermal strengthening, including NH_3 , which was broadly used as ORR composite. However, strict constraints or special tools are usually needed for this method. Thus, creating metal-free catalysts with better

performance, cost-effectiveness, strong stability, and gentle essentials stays a hurdle.^[109]

Niu et al.^[110] proposed positively sturdy N-doped CNTs emanated by CDs and MOFs to superior, effective electrocatalyst toward ORR. Figure 12a illustrates a diagram of N-CNTs derived from N-CDs and MOFs for positively effective material of ORR. Within Figure 12b, ZIF-67 prototypes were developed within homogenous rod-like atoms with an exposed end. Precisely equivalent to the bottom-up organic process, this is clear from the bigger particles with a turbulent formation, wherever the ZIF-67 dodecahedron was finally transformed within thin N-CNTs with N-CDs through the pyrolysis method. An intermediate width of around 15 nm was measured for the as-synthesized N-CNTs, as illustrated in Figure 12c. Figure 12d shows HRTEM pictures of complicated organizational details and the atomic lattice edges of N-CNTs. Interlayer arrangement of graphite (002) along with the matrix space, which is around 0.311 nm, is illustrated in Figure 12e. During the matrix space ($\approx 0.205 \text{ nm}$) it is also constant through the Co (111) facade, as illustrated in Figure 12f.

As earlier said, it is expected that the designed N-CNTs can be employed as fuel cells and metal–air batteries as they can show notable ORR catalytic performance within rechargeable appliances. Thus, CV measures evaluate the ORR electrocatalytic performance. For the comparison, unadorned glassy carbon electrode (GCE), N-CDs, Co–N–C nanohybrids and viability known Pt/C catalysts were also strained below the identical circumstances. Figure 12g shows the CVs for N_2 - and O_2 -saturated N-CNT electrodes into 0.1 M KOH on a sweep rate of 10 mV s^{-1} . To additionally explain the part of N-CNTs within ORR, LSV measures were documented upon a rotating disk electrode (RDE) within an O_2 -pervaded alkaline solution at a spinning speed of 1600 rpm. In contrast, ORR polarization curves were also received for N-CDs, unmodified GCE, traditionally known as Pt/C and Co–N–C nanohybrids probes. As shown in Figure 12h, in comparison with GCE, N-CDs, and Co–N–C nanohybrids probes, the initial voltage ($E_0 = 0.88 \text{ V}$) and half-wave voltage ($E_{1/2} = 0.82 \text{ V}$) of N-CNTs are significantly more favorable. Also, to thoroughly comprehend the electron transfer tool concerned with the activity of ORR, the ORR polarization plots on special rotating rates (ω) were examined in the segment. As demonstrated in Figure 12i, the limiting current density (j_L) grows with higher spinning speeds toward all materials because of the condensed scattering extent at higher rates. In Figure 12j, significances of n within the current investigation change for N-CDs and Co–N–C nanohybrids between voltage ranges of 1.3 and 1.7 that lead to overwhelmed ORR two-electron approaches with HO_2^- upon the electrode. Consequently, the j_K significance of N-CNTs may acquire 8.10 mA cm^{-2} on 0.3 V, which is 2.2-folds higher than N-CDs, 1.6 times more extensive than Co–N–C nanohybrids, and 1.3 times more significant compared with Pt/C, as shown in Figure 12k, correspondingly. In addition, the Tafel plot is an essential element to consider catalytic performance. Consequently, the slant of N-CNTs ($\approx 81 \text{ mV dec}^{-1}$) can be seen as lower compared with the Pt/C composite ($\approx 132 \text{ mV dec}^{-1}$), as illustrated in Figure 12l; this indicates the quick kinetics of N-CNTs. Consequently, the $4e^-$ ORR method shows that N-CNTs deliver excellent catalytic performance.

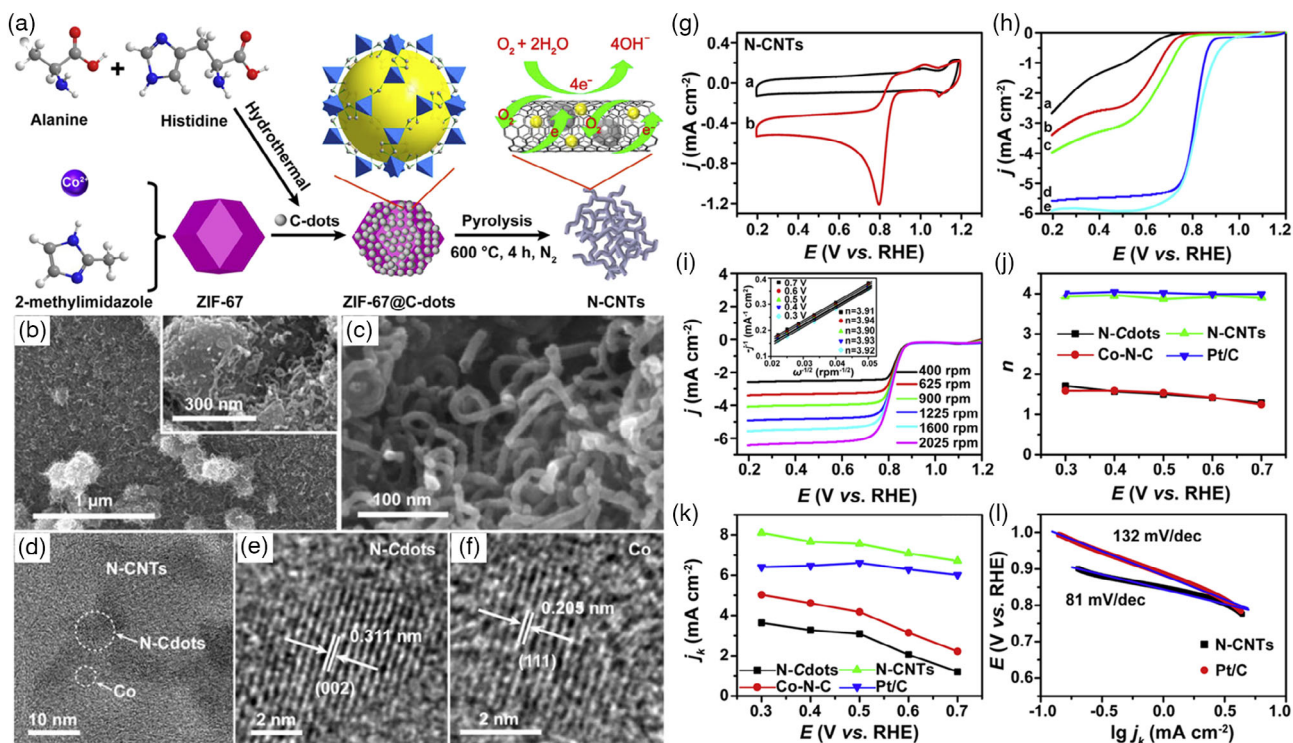


Figure 12. a) Graphic representation of positively efficient N-doped CNT electrocatalyst that emanated from CDs and MOFs for ORR. b) Low-resolution, c) HR SEM pictures, d–f) HRTEM pictures. g) CVs for N-CNT electrodes within N_2 -saturated and O_2 -saturated alkaline media at a sweep speed of 10 mV s^{-1} . h) The LSV curves for unmodified a) GCE, b) N-CDs, c) Co–N–C nano hybrids, d) nitrogen-doped CNTs, and e) probes of Pt/C at 1600 rpm within O_2 -saturated alkaline media, including a sweep speed of 5 mV s^{-1} . i) LSVs of N-CNTs probe within O_2 -saturated alkaline media on a succession of process rates as 400–2025 rpm, including a sweep speed of 5 mV s^{-1} . Inset shows the K – L slopes of N-CNTs at distinct voltages. j) Reliance of electron transfer numeral and k) kinetic current density as the operation of voltages toward N-CDs, Co–N–C nano hybrids, N-CNTs, and Pt/C probe in O_2 -saturated 0.1 M KOH, correspondingly. l) Tafel slopes of N-CNTs and Pt/C where Tafel plots were estimated through a linear reversion approach. Reprinted with permission.^[110] Copyright 2019, Elsevier Ltd.

Further, Table 2 shows the applications and different important parameters of CD-based materials in water splitting.

4.4. Electromagnetic Interference Absorption/Shielding

Carbonaceous byproducts within the previous years have yielded excellent concentration for the design of functioning catalysts owing to their QD surface characteristics, ultrathin organizational component, notably better strength-to-weight proportion, anticorrosion characteristics, exceptional transporter mobility ($\approx 200\,000 \text{ cm}^2 \text{ V}^{-1} \text{ s}$), and significantly better thermal conductivity (around $5300 \text{ W m}^{-1} \text{ K}$).^[123] Hybrid materials possessing carbonaceous inclusions usually work as more suitable shielding composites toward their lightweight, high specific exterior area, and flexibility and earlier noted electronic features.^[124] CNSs, CNTs, Gr, and Gr byproducts are broadly investigated^[125] and also examine how they affect EM absorption/EMI shielding in core–shell system characteristics.

Singh et al.^[126] reported CdSe@V2O5 core–shell QDs with reduced GO (rGO–V–CdSe) to design a light EMI shielding substance. A solvothermal method was utilized to prepare this core–shell design. This system’s increased dielectric failure and protecting efficacy were attributed to different defects that exist in it,

which showed dipolar and interfacial polarization. Complete protecting efficacy up to $\approx 38 \text{ dB}$ has been documented within the X band.

4.5. Solar-Assisted Energy Generation

Global warming, mainly driven by CO_2 emission from the ignition of fossil fuels, is anticipated to have overwhelming effects on the Earth. The lessening of CO_2 emission and the quest toward hygienic and bearable options for fossil fuels are thus attractive and incredibly critical, particularly under the very enterprising international environment guidelines for the phase-down of coal usage. Hydrogen (H_2), a universal energy conveyance, is regarded as one of the most favorable origins of pure energy to attack multiple energy hurdles and has newly acquired exceptional awareness globally owing to its highly gravimetric energy density, about negligible greenhouse gas emissions properties, and ability to be utilized for living manufacturing set-up or power factories powered through fossil fuels.^[127]

The manufactured process of MXene-derived monodots (MXDs), CQDs, and the MXene@carbon(MX@C) mixture is schematically shown in Figure 13a. Shortly, CQDs were manufactured through a bottom-up process based upon hydrothermal removal at 200°C utilizing fumaronitrile as the carbon origin

Table 2. Applications of CD-based materials in water splitting.

[CD]-based nanomaterials ^{a)}	Preparation method	Overpotential	Surface area [m ² g ⁻¹]	Pore size [nm]	Faradic efficiency [%]	Technique used	Activity	Ref.
Co(OH) ₂ @NCDs	In situ hydrothermal method	296 mV at 10 A cm ⁻²	19.4	1.66	100	LSV	OER	[111]
CD/MOF	Solvothermal method	320 mV at 10 mV cm ⁻²	59.80	19.43	–	CV	OER	[94]
PANI/CDs	Centrifugation	150 mV at 30 mA cm ⁻² 65 at 20 ma cm ⁻²	–	–	90	CV and LSV	OER HER	[112]
CoP-NCDs/NF	Hydrothermal and calcination	103 mV 226 mV at 10 mA cm ⁻²	158.66	–	–	CV	HER OER	[113]
gC ₃ N ₄ /NCDs/WO _x	Solvothermal method	–	333.89	3.6	–	EIS	HER	[114]
N-C@CoNPs	One-pot hydrothermal method	137 mV at 10 mA cm ⁻² 353 mV at 10 mA cm ⁻²	150.796	–	–	CV	HER OER	[115]
RuCo@CD	Rational modification	11 mV 190 mV at 10 mA cm ⁻²	135.6	41.26	–	EIS	HER OER	[116]
CDs/NiCo ₂ S ₄ /Ni ₃ S ₂ /NF	Hydrothermal and ion exchange method	1.5 V at 10 mA cm ⁻²	–	–	–	LSV	HER OER	[117]
Ru@CDs	Hydrothermal and pyrolysis	30 mV at 10 mA cm ⁻²	–	–	–	EIS	HER	[118]
CD/CoNi	Hydrothermal	–324 mV at 10 mA cm ⁻²	48.071	3.6	–	LSV	HER	[119]
SO ₃ -CDs/NiFe LDH	Hydrothermal method	200 mV at 10 mA cm ⁻²	146.9	–	97.5	LSV	OER	[101]
N-CQDs	One-pot reflux-assisted polymerization	522 mV at 10 mA cm ⁻²	–	3.0	–	LSV	HER	[120]
N-doped and defect-containing MoP/CDs	Pyrolysis	70 mV at 10 mA cm ⁻²	755.5	2.8	–	EIS	HER	[91]
Sulfur-doped NiCo/CDs	–	232 mV at 10 mA cm ⁻²	–	–	–	LSV	HER	[121]
CDs/Pt-PANI)	Electrochemical polymerization	30 mV at 10 mA cm ⁻²	–	–	–	EIS	HER	[122]

^{a)}CoP-NCDs/NF: fungus-like CoP-NCD/ Ni foam; gC₃N₄ /NCDs/WO_x: graphitic carbon nitride/NCD/tin oxide; NP: Nanoparticle; NiFe LDH: Nickel–iron layered double hydroxide; MoP: Molybdenum phosphate.

for 20 min. The surface and microstructure of the pure and mixed nanodots were investigated via TEM, as illustrated in Figure 13b–c. MXDs and CQDs have almost spherical and oblate shapes (Figure 13b,c), showing no apparent cluster with the typical atom dimensions of 7.3 and 2.6 nm separately. Figure 13d illustrates the core–shell-designed MX@C amalgam nanodots at a shell consistency of ≈1.6 nm. The optic and electronic characteristics were examined through UV–vis and PL spectrometry, as illustrated in Figure 13e,f. The physically miscellaneous CQD and MXD (CQD-MXD) were used as control specimens. Figure 13g demonstrates the LSV arcs within 1 M KOH solution at a pH of 14 after IR recompense. Tafel slope, log (|j|) versus η was used to confirm the catalytical performance of the HER. A shorter Tafel plot shows that a lower η is needed for the composite to reach the desired current. As shown in Figure 13h, the Tafel plot of MX@C was 32 mV dec⁻¹ and more inferior compared with pure MXD (49 mV dec⁻¹), CQD (46 mV dec⁻¹), and CQD-MXD (35 mV dec⁻¹). Furthermore, we corresponded the η of composites at 10 and 100 mA cm⁻², as illustrated in Figure 13i. 205 and 328 mV were η for the MX@C mixture, lesser as compared with the CQDs, MXDs, and CQD-MXD at 10 and 100 mA cm⁻². As demonstrated in Figure 13j, Nyquist slops for MX@C hybrid at the open-circuit voltage exhibit an

inferior charge transfer resistance (79 Ω) than those of additional nanodots, reducing the charge transportation performance toward the improved HER movement. In contrast, the MX@C hybrid composite operates virtually and is positively involved at all pH ranges, as illustrated in Figure 13k. Electrochemical stability is an influential factor in evaluating that an electrocatalyst shows HER activity. Therefore, the cycling stability of CQD-MXD and MX@C was conducted over 1000 runs, utilizing constant CV within an alkaline media, as demonstrated in Figure 13L.^[128]

5. Conclusion, Challenges, and Outlook

This study suggests various kinds and synthesis techniques of CDs and their implementations as electrode substances in EES (such as SCs and batteries) and electroactive materials of HER, OER, and ORR into water oxidation cells, EMI shielding, and fuel cells. These study results indicate that CDs are among the multiple-competent NMs with conspicuous characteristics: considerable specific exterior area, flexible nanoscale dimensions, quick electron transfer capability, quantum dimension consequence, large exterior practical groups, and different defects that ensure their significant potential within EES applications.

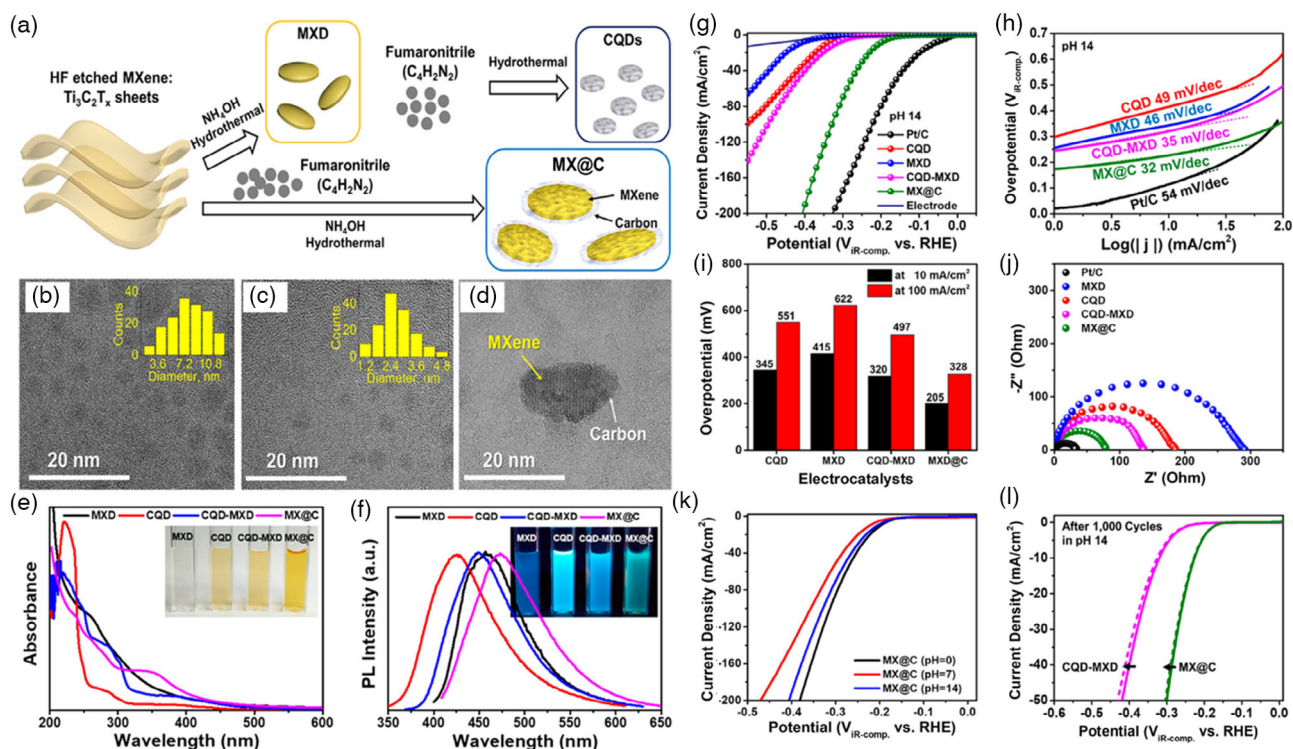


Figure 13. a) Graphic description of the preparation of MXDs, CQDs, MX@C, and CQD-MXD. TEM pictures of b) MXDs, c) CQDs, and d) MX@C. Insets of (b) and (c) demonstrate particle extent delivery histograms of MXDs and CQDs. e) UV-vis spectrum and f) standardized PL spectrum on a static excited wavelength of 360 nm of MXDs, CQDs, CQD-MXD, and MX@C media. Insets of (e) and (f) display digital photos of MXDs, CQDs, CQD-MXD, and MX@C media below visible rays and UV light (365 nm). g) HER polarization arcs and h) Tafel slopes for retail Pt/C, MXDs, CQDs, CQD-MXD, and MX@C composites within 1 M KOH with recompense. i) Relative η at different current densities and j) Nyquist slopes of retail Pt/C, MXDs, CQDs, CQD-MXD, and MX@C probes. k) Polarization arcs of MX@C at pH 0, 7, and 14. l) Stability examination at pH 14 for CQD-MXD and MX@C after 1000 CV runs. Reprinted with permission.^[128] Copyright 2020, American Chemical Society.

CDs may work as electron contributors and acceptors. This distinctive essence has also created perfect catalysts within other catalytic responses, such as photocatalysis, electrocatalytic O₂ or CO₂ removal, and overall water splitting. Most of the CDs-dependent catalysts with high catalytic performance are present within the structure of CD-metal composites. Higher catalytic performance is anticipated via advanced synthesis processes and a profound acquaintance of the synergistic tool among metal and CDs into various catalytic responses. In contrast, economic CD-based nanomaterials catalysts can substitute the retail Pt/C catalyst within a few specific reactions (such as electrocatalytic O₂ deduction), and superior performance may be acquired by sensible reasoning structural composition and structural constraint. In addition, bare CDs should usually be incorporated (like heat processing) before being utilized as electrocatalysts within aqueous media to evade accumulating and liquifying.

Finally, CDs have demonstrated outstanding prospects toward EES and catalysis implementations, although far from being ultimately used. Continued study and growth of controllable synthesis techniques and attaining a more reasonable interpretation of the connection among their design and arrangements and their functional tools as the EES substances and electrocatalysts are required. In this respect, few in situ depictions of CD-based composites and their operating mechanisms during the EES and

electrocatalysis methods should be utilized for essential acquaintance and growth of unique substances. Indeed, this may be considered that these distinctively outstanding components of CDs will prompt more exciting developments in the upcoming future.

Acknowledgements

The authors acknowledge support from the Department of Chemistry and Research & Development Cell of Maharishi Markandeshwar (Deemed to be University), Mullana, Ambala, Haryana, India. V.K.T. would also like to thank the research support provided by the UKRI via grant no. EP/T024607/1, Royal Academy of Engineering (IAPP18-19\295), and SFC (UIF funding).

Conflict of Interest

The authors declare no conflict of interest.

Keywords

batteries, carbon dots, electrocatalysts, electromagnetic interference shielding, oxygen/hydrogen evolution reactions, supercapacitors

Received: April 26, 2022

Revised: May 24, 2022

Published online:

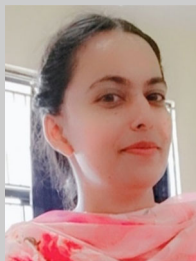
- [1] a) A. Tyagi, M. C. Joshi, A. Shah, V. K. Thakur, R. K. Gupta, *ACS Omega* **2019**, *4*, 3257; b) S. D. Mahapatra, P. C. Mohapatra, A. I. Aria, G. Christie, Y. K. Mishra, S. Hofmann, V. K. Thakur, *Adv. Sci.* **2021**, *8*, 2100864; c) V. K. Thakur, *Nanomaterials* **2020**, *10*, 1800; d) S. Chen, A. Skordos, V. K. Thakur, *Mater. Today Chem.* **2020**, *17*, 100304.
- [2] a) L. Dai, D. W. Chang, J.-B. Baek, W. Lu, *Small* **2012**, *8*, 1130; b) T. Tang, L. Ding, Z. Jiang, J.-S. Hu, L.-J. Wan, *Sci. China Chem.* **2020**, *63*, 1517; c) K. Sheoran, H. Kaur, S. S. Siwal, A. K. Saini, D.-V. N. Vo, V. K. Thakur, *Chemosphere* **2022**, *299*, 134364; d) A. Muhulet, F. Miculescu, S. I. Voicu, F. Schütt, V. K. Thakur, Y. K. Mishra, *Mater. Today Energy* **2018**, *9*, 154.
- [3] P. Wu, Y. Xu, J. Zhan, Y. Li, H. Xue, H. Pang, *Small* **2018**, *14*, 1801479.
- [4] a) X. Li, M. Rui, J. Song, Z. Shen, H. Zeng, *Adv. Funct. Mater.* **2015**, *25*, 4929; b) M. Semeniuk, Z. Yi, V. Poursorkhabi, J. Tjong, S. Jaffer, Z.-H. Lu, M. Sain, *ACS Nano* **2019**, *13*, 6224; c) Q. Xia, W. Zeng, F. Ji, X. Chen, Y. Zhang, F. Ling, W. Hu, L. Fang, S. N. Khisro, M. Zhou, *J. Mater. Chem. C* **2019**, *7*, 11441.
- [5] Y. Pang, J. Wei, Y. Wang, Y. Xia, *Adv. Energy Mater.* **2018**, *8*, 1702288.
- [6] H. Lv, Y. Yuan, Q. Xu, H. Liu, Y.-G. Wang, Y. Xia, *J. Power Sources* **2018**, *398*, 167.
- [7] K. Mishra, V. K. Thakur, S. S. Siwal, *Mater. Today: Proc.* **2022**, *56*, 107.
- [8] J. Sun, Y. Liu, Z. Wu, M. Xu, *Carbohydr. Polym.* **2021**, *252*, 117209.
- [9] H. Wu, M. Wu, B. Wang, X. Yong, Y. Liu, B. Li, B. Liu, S. Lu, *J. Energy Chem.* **2020**, *48*, 43.
- [10] Y. Liu, X. Li, Q. Zhang, W. Li, Y. Xie, H. Liu, L. Shang, Z. Liu, Z. Chen, L. Gu, Z. Tang, T. Zhang, S. Lu, *Angew. Chem. Int. Ed.* **2020**, *59*, 1718.
- [11] B. Wang, S. Lu, *Matter* **2022**, *5*, 110.
- [12] Y. Liu, S. Roy, S. Sarkar, J. Xu, Y. Zhao, J. Zhang, *Carbon Energy* **2021**, *3*, 795.
- [13] Y. Zhai, B. Zhang, R. Shi, S. Zhang, Y. Liu, B. Wang, K. Zhang, G. I. N. Waterhouse, T. Zhang, S. Lu, *Adv. Energy Mater.* **2022**, *12*, 2103426.
- [14] R. Cheng, Y. Xiang, R. Guo, L. Li, G. Zou, C. Fu, H. Hou, X. Ji, *Small* **2021**, *17*, 2102091.
- [15] a) S. S. Siwal, A. K. Saini, S. Rarotra, Q. Zhang, V. K. Thakur, *J. Nanostruct. Chem.* **2021**, *11*, 93; b) S. Karamveer, V. K. Thakur, S. S. Siwal, *Mater. Today: Proc.* **2022**, *56*, 9; c) S. S. Siwal, Q. Zhang, N. Devi, K. V. Thakur, *Polymers* **2020**, *12*, 505.
- [16] W. Liang, C. E. Bunker, Y.-P. Sun, *ACS Omega* **2020**, *5*, 965.
- [17] R. Cheng, M. Jiang, K. Li, M. Guo, J. Zhang, J. Ren, P. Meng, R. Li, C. Fu, *Chem. Eng. J.* **2021**, *425*, 130603.
- [18] a) K. J. Mintz, Y. Zhou, R. M. Leblanc, *Nanoscale* **2019**, *11*, 4634; b) F. Yan, Y. Jiang, X. Sun, Z. Bai, Y. Zhang, X. Zhou, *Microchim. Acta* **2018**, *185*, 424.
- [19] K. J. Mintz, M. Bartoli, M. Rovere, Y. Zhou, S. D. Hettiarachchi, S. Paudyal, J. Chen, J. B. Domena, P. Y. Liyanage, R. Sampson, D. Khadka, R. R. Pandey, S. Huang, C. C. Chusuei, A. Tagliaferro, R. M. Leblanc, *Carbon* **2021**, *173*, 433.
- [20] P. Zuo, X. Lu, Z. Sun, Y. Guo, H. He, *Microchim. Acta* **2016**, *183*, 519.
- [21] J. Peng, W. Gao, B. K. Gupta, Z. Liu, R. Romero-Aburto, L. Ge, L. Song, L. B. Alemany, X. Zhan, G. Gao, S. A. Vithayathil, B. A. Kaiparettu, A. A. Marti, T. Hayashi, J.-J. Zhu, P. M. Ajayan, *Nano Letters, J. Mater. Chem.* **2012**, *2012*, 8764.
- [22] Y. Li, Y. Hu, Y. Zhao, G. Shi, L. Deng, Y. Hou, L. Qu, *Adv. Mater.* **2011**, *23*, 776.
- [23] L. Lin, S. Zhang, *Chem. Commun.* **2012**, *48*, 10177.
- [24] L.-L. Li, J. Ji, R. Fei, C.-Z. Wang, Q. Lu, J.-R. Zhang, L.-P. Jiang, J.-J. Zhu, *Adv. Funct. Mater.* **2012**, *22*, 2971.
- [25] M. Bottini, C. Balasubramanian, M. I. Dawson, A. Bergamaschi, S. Bellucci, T. Mustelin, *J. Phys. Chem. B* **2006**, *110*, 831.
- [26] L. A. Ponomarenko, F. Schedin, M. I. Katsnelson, R. Yang, E. W. Hill, K. S. Novoselov, A. K. Geim, *Science* **2008**, *320*, 356.
- [27] Y.-P. Sun, B. Zhou, Y. Lin, W. Wang, K. A. S. Fernando, P. Pathak, M. J. Mezzani, B. A. Harruff, X. Wang, H. Wang, P. G. Luo, H. Yang, M. E. Kose, B. Chen, L. M. Veca, S.-Y. Xie, *J. Am. Chem. Soc.* **2006**, *128*, 7756.
- [28] L. Fan, M. Zhu, X. Lee, R. Zhang, K. Wang, J. Wei, M. Zhong, D. Wu, H. Zhu, *Particle Particle Syst. Character.* **2013**, *30*, 764.
- [29] X. Yan, X. Cui, B. Li, *Nano Lett.* **2010**, *10*, 1869.
- [30] L. Tang, R. Ji, X. Cao, J. Lin, H. Jiang, X. Li, K. S. Teng, C. M. Luk, S. Zeng, J. Hao, S. P. Lau, *ACS Nano* **2012**, *6*, 5102.
- [31] X. Yan, X. Cui, L. S. Li, *J. Am. Chem. Soc.* **2010**, *132*, 5944.
- [32] J. Zhou, H. Zhou, J. Tang, S. Deng, F. Yan, W. Li, M. Qu, *Microchim. Acta* **2017**, *184*, 343.
- [33] a) F. Li, T. Li, C. Sun, J. Xia, Y. Jiao, H. Xu, *Angew. Chem. Int. Ed.* **2017**, *56*, 9910; b) M. Sudolská, M. Dubecký, S. Sarkar, C. J. Reckmeier, R. Zbořil, A. L. Rogach, M. Otyepka, *J. Phys. Chem. C* **2015**, *119*, 13369.
- [34] K. K. Chan, S. H. K. Yap, K.-T. Yong, *Nano-Micro Lett.* **2018**, *10*, 72.
- [35] X. Sun, Y. Lei, *Trends Anal. Chem.* **2017**, *89*, 163.
- [36] S.-L. Hu, K.-Y. Niu, J. Sun, J. Yang, N.-Q. Zhao, X.-W. Du, *J. Mater. Chem.* **2009**, *19*, 484.
- [37] S. Qu, X. Wang, Q. Lu, X. Liu, L. Wang, *Angew. Chem. Int. Ed.* **2012**, *51*, 12215.
- [38] C. Wang, Z. Xu, H. Cheng, H. Lin, M. G. Humphrey, C. Zhang, *Carbon* **2015**, *82*, 87.
- [39] Y. Dong, R. Wang, H. Li, J. Shao, Y. Chi, X. Lin, G. Chen, *Carbon* **2012**, *50*, 2810.
- [40] a) M. Ganiga, J. Cyriac, *Sens. Actuators B: Chem.* **2016**, *225*, 522; b) C. Han, R. Wang, K. Wang, H. Xu, M. Sui, J. Li, K. Xu, *Biosens. Bioelectron.* **2016**, *83*, 229.
- [41] R. K. Das, S. Mohapatra, *J. Mater. Chem. B* **2017**, *5*, 2190.
- [42] Y. Wang, A. Hu, *J. Mater. Chem. C* **2014**, *2*, 6921.
- [43] S. Anwar, H. Ding, M. Xu, X. Hu, Z. Li, J. Wang, L. Liu, L. Jiang, D. Wang, C. Dong, M. Yan, Q. Wang, H. Bi, *ACS Appl. Bio Mater.* **2019**, *2*, 2317.
- [44] J. Liu, R. Li, B. Yang, *ACS Central Sci.* **2020**, *6*, 2179.
- [45] B. D. Mansuriya, Z. Altintas, *Nanomaterials* **2021**, *11*, 2525.
- [46] L. Cui, X. Ren, M. Sun, H. Liu, L. Xia, *Nanomaterials* **2021**, *11*, 3419.
- [47] X. Xu, R. Ray, Y. Gu, H. J. Ploehn, L. Gearheart, K. Raker, W. A. Scrivens, *J. Am. Chem. Soc.* **2004**, *126*, 12736.
- [48] X. Wang, L. Cao, S.-T. Yang, F. Lu, M. J. Mezzani, L. Tian, K. W. Sun, M. A. Bloodgood, Y.-P. Sun, *Angew. Chem. Int. Ed.* **2010**, *49*, 5310.
- [49] R. Guo, L. Li, B. Wang, Y. Xiang, G. Zou, Y. Zhu, H. Hou, X. Ji, *Energy Storage Mater.* **2021**, *37*, 8.
- [50] a) S. S. Siwal, Q. Zhang, C. Sun, V. K. Thakur, *Nanomaterials* **2019**, *10*, 2; b) M. Choudhary, S. Siwal, D. Nandi, K. Mallick, *Appl. Surf. Sci.* **2017**, *424*, 151.
- [51] a) C. Liu, Z. Yu, D. Neff, A. Zhamu, B. Z. Jang, *Nano Letters*, *10*, 4863; b) T. Chen, L. Dai, *J. Mater. Chem. A* **2010**, *2014*, 10756.
- [52] I. Shown, A. Ganguly, L.-C. Chen, K.-H. Chen, *Energy Sci. Eng.* **2015**, *3*, 2.
- [53] a) S. N. Baker, G. A. Baker, *Angew. Chem. Int. Ed.* **2010**, *49*, 6726; b) L. Wang, X. Chen, Y. Lu, C. Liu, W. Yang, *Carbon*, **2015**, *94*, 472.
- [54] a) D. Tian, C. Wang, X. Lu, *Adv. Energy Sustain. Res.* **2021**, *2*, 2100024; b) L. Wang, X. Zhang, Y. Xu, C. Li, W. Liu, S. Yi, K. Wang, X. Sun, Z.-S. Wu, Y. Ma, *Adv. Funct. Mater.* **2021**, *31*, 2104286; c) S. Yi, L. Wang, X. Zhang, C. Li, W. Liu, K. Wang, X. Sun, Y. Xu, Z. Yang, Y. Cao, J. Sun, Y. Ma, *Sci. Bull.* **2021**, *66*, 914; d) C. Li, X. Zhang,

- Z. Lv, K. Wang, X. Sun, X. Chen, Y. Ma, *Chem. Eng. J.* **2021**, 414, 128781; e) Y. An, T. Liu, C. Li, X. Zhang, T. Hu, X. Sun, K. Wang, C. Wang, Y. Ma, *J. Mater. Chem. A* **2021**, 9, 15654; f) J. Sun, B. Luo, H. Li, *Adv. Energy Sustain. Res.* **2022**, n/a, 2100191; g) S.-H. Jiang, J. Ding, R.-H. Wang, F.-Y. Chen, J. Sun, Y.-X. Deng, X.-L. Li, *Rare Metals* **2021**, 40, 3520.
- [55] X. Zhang, J. Wang, J. Liu, J. Wu, H. Chen, H. Bi, *Carbon* **2017**, 115, 134.
- [56] B. Unnikrishnan, C.-W. Wu, I. W. P. Chen, H.-T. Chang, C.-H. Lin, C.-C. Huang, *ACS Sustain. Chem. Eng.* **2016**, 4, 3008.
- [57] Z. Zhao, Y. Xie, *J. Power Sources* **2017**, 337, 54.
- [58] S. Mondal, U. Rana, S. Malik, *Chem. Commun.* **2015**, 51, 12365.
- [59] X. Jian, J.-g. Li, H.-m. Yang, L.-l. Cao, E.-h. Zhang, Z.-h. Liang, *Carbon* **2017**, 114, 533.
- [60] J.-S. Wei, H. Ding, P. Zhang, Y.-F. Song, J. Chen, Y.-G. Wang, H.-M. Xiong, *Small* **2016**, 12, 5927.
- [61] J.-S. Wei, C. Ding, P. Zhang, H. Ding, X.-Q. Niu, Y.-Y. Ma, C. Li, Y.-G. Wang, H.-M. Xiong, *Adv. Mater.* **2019**, 31, 1806197.
- [62] W. Pholauyphon, R. N. Bulakhe, J. Praneerad, R. Attajak, J. Manyam, I. In, P. Paoprasert, *Electrochim. Acta* **2021**, 390, 138805.
- [63] L. Yu, C.-T. Hsieh, D. J. Keffer, H. Chen, G. A. Goenaga, S. Dai, T. A. Zawodzinski, D. P. Harper, *ACS Omega* **2021**, 6, 7851.
- [64] L. Song, C. Peng, F. Yang, L. Wang, Y. Jiang, Y. Wang, *ACS Appl. Energy Mater.* **2021**, 4, 4654.
- [65] C. Liu, Z. Zhao, Y. Liu, Q. Lu, *J. Power Sources* **2022**, 519, 230780.
- [66] Z. Ji, K. Liu, W. Dai, D. Ma, H. Zhang, X. Shen, G. Zhu, S. Wu, *Nanoscale* **2021**, 13, 1689.
- [67] W. Luo, W. Zeng, H. Quan, M. Pan, Y. Wang, D. Chen, *J. Alloys Compd.* **2021**, 868, 159048.
- [68] L. Cui, Y. An, H. Xu, M. Jia, Y. Li, X. Jin, *N. J. Chem.* **2021**, 45, 21692.
- [69] Q. Li, H. Cheng, X. Wu, C.-F. Wang, G. Wu, S. Chen, *J. Mater. Chem. A* **2018**, 6, 14112.
- [70] Z. Ji, K. Liu, N. Li, H. Zhang, W. Dai, X. Shen, G. Zhu, L. Kong, A. Yuan, *J. Colloid Interface Sci.* **2020**, 579, 282.
- [71] F. Xie, M. Zhou, G. Wang, Q. Wang, M. Yan, H. Bi, *Int. J. Energy Res.* **2019**, 43, 7529.
- [72] Z. Ji, N. Li, M. Xie, X. Shen, W. Dai, K. Liu, K. Xu, G. Zhu, *Electrochim. Acta* **2020**, 334, 135632.
- [73] R. M. A. P. Lima, H. P. de Oliveira, *J. Energy Storage* **2020**, 28, 101284.
- [74] Z. Ji, W. Dai, S. Zhang, G. Wang, X. Shen, K. Liu, G. Zhu, L. Kong, J. Zhu, *Adv. Powder Technol.* **2020**, 31, 632.
- [75] S. Li, A. Gao, F. Yi, D. Shu, H. Cheng, X. Zhou, C. He, D. Zeng, F. Zhang, *Electrochim. Acta* **2019**, 297, 1094.
- [76] P. Zhang, L. Li, D. Nordlund, H. Chen, L. Fan, B. Zhang, X. Sheng, Q. Daniel, L. Sun, *Nat. Commun.* **2018**, 9, 381.
- [77] J.-Q. Chi, K.-L. Yan, Z. Xiao, B. Dong, X. Shang, W.-K. Gao, X. Li, Y.-M. Chai, C.-G. Liu, *Int. J. Hydrogen Energy* **2017**, 42, 20599.
- [78] M. Sadaqat, L. Nisar, N.-U.-A. Babar, F. Hussain, M. N. Ashiq, A. Shah, M. F. Ehsan, M. Najam-Ul-Haq, K. S. Joya, *J. Mater. Chem. A* **2019**, 7, 26410.
- [79] B. K. Barman, K. K. Nanda, *Dalton Trans.* **2016**, 45, 6352.
- [80] L. Jin, H. Pang, *Chin. Chem. Lett.* **2020**, 31, 2300.
- [81] S. S. Siwal, W. Yang, Q. Zhang, *J. Energy Chem.* **2020**, 51, 113.
- [82] L. Wang, X. Wu, S. Guo, M. Han, Y. Zhou, Y. Sun, H. Huang, Y. Liu, Z. Kang, *J. Mater. Chem. A* **2017**, 5, 2717.
- [83] P. Chandrasekaran, T. N. J. I. Edison, M. G. Sethuraman, *Int. J. Hydrogen Energy* **2020**, 45, 28800.
- [84] S. Lu, L. Sui, J. Liu, S. Zhu, A. Chen, M. Jin, B. Yang, *Adv. Mater.* **2017**, 29, 1603443.
- [85] S. Lu, L. Sui, Y. Liu, X. Yong, G. Xiao, K. Yuan, Z. Liu, B. Liu, B. Zou, B. Yang, *Adv. Sci.* **2019**, 6, 1801470.
- [86] W. Li, Y. Liu, B. Wang, H. Song, Z. Liu, S. Lu, B. Yang, *Chin. Chem. Lett.* **2019**, 30, 2323.
- [87] B. Wang, J. Li, Z. Tang, B. Yang, S. Lu, *Sci. Bull.* **2019**, 64, 1285.
- [88] D. Qu, J. Liu, X. Miao, M. Han, H. Zhang, Z. Cui, S. Sun, Z. Kang, H. Fan, Z. Sun, *Appl. Catal. B: Environ.* **2018**, 227, 418.
- [89] a) Y. Liu, Y. Yang, Z. Peng, Z. Liu, Z. Chen, L. Shang, S. Lu, T. Zhang, *Nano Energy*, **2019**, 65, 104023; b) W. Yang, J. Zeng, Y. Hua, C. Xu, S. S. Siwal, Q. Zhang, *J. Power Sources* **2019**, 436, 226887.
- [90] a) W. Li, Z. Wei, B. Wang, Y. Liu, H. Song, Z. Tang, B. Yang, S. Lu, *Mater. Chem. Front.* **2020**, 4, 277; b) J. Zeng, J. Liu, S. S. Siwal, W. Yang, X. Fu, Q. Zhang, *Appl. Surf. Sci.* **2019**, 491, 570.
- [91] H. Song, Y. Li, L. Shang, Z. Tang, T. Zhang, S. Lu, *Nano Energy* **2020**, 72, 104730.
- [92] Q. Qin, H. Jang, L. Chen, G. Nam, X. Liu, J. Cho, *Adv. Energy Mater.* **2018**, 8, 1801478.
- [93] H. Song, Y. Cheng, B. Li, Y. Fan, B. Liu, Z. Tang, S. Lu, *ACS Sustain. Chem. Eng.* **2020**, 8, 3995.
- [94] M. Y. u. Rehman, S. Manzoor, N. Nazar, A. G. Abid, A. M. Qureshi, A. H. Chughtai, K. S. Joya, A. Shah, M. N. Ashiq, *J. Alloys Compd.* **2021**, 856, 158038.
- [95] M. Zhu, Y. Zhou, Y. Sun, C. Zhu, L. Hu, J. Gao, H. Huang, Y. Liu, Z. Kang, *Dalton Trans.* **2018**, 47, 5459.
- [96] a) F. Yan, Y. Zou, M. Wang, X. Mu, N. Yang, L. Chen, *Sens. Actuators B: Chem.* **2014**, 192, 488; b) A. Mary Alex, M. D. Kiran, G. Hari, A. Krishnan, J. S. Jayan, A. Saritha, *Mater. Today: Proc.* **2020**, 26, 716.
- [97] T. Bao, L. Song, S. Zhang, *Chem. Eng. J.* **2018**, 351, 189.
- [98] X. Kou, X. Xin, Y. Zhang, L.-Y. Meng, *Carbon Lett.* **2021**, 31, 695.
- [99] a) S. S. Narwade, S. M. Mali, R. V. Digraaskar, V. S. Sapner, B. R. Sathe, *Int. J. Hydrogen Energy* **2019**, 44, 27001; b) Y. Dong, J. Yang, Y. Liu, Y. Wang, Z. Dong, M. Cui, M. Li, X. Yuan, X. Zhang, X. Dai, *Dalton Trans.* **2020**, 49, 6355.
- [100] a) A. Roy, A. Ray, S. Saha, M. Ghosh, T. Das, B. Satpati, M. Nandi, S. Das, *Electrochim. Acta* **283**, 327; b) P. Chaudhary, P. P. Ingole, *Int. J. Hydrogen Energy* **2018**, 2020, 45, 16060.
- [101] W. Zhu, S. Chen, F. Liao, X. Zhao, H. Shi, Y. Shi, L. Xu, Q. Shao, Z. Kang, M. Shao, *Chem. Eng. J.* **2021**, 420, 129690.
- [102] a) C. Sealy, *Mater. Today* **2008**, 11, 65; b) M. Shao, Q. Chang, J.-P. Dodelet, R. Chenitz, *Chem. Rev.* **2016**, 116, 3594.
- [103] a) L. Dai, Y. Xue, L. Qu, H.-J. Choi, J.-B. Baek, *Chem. Rev.* **2015**, 115, 4823; b) X. Liu, L. Dai, *Nat. Rev. Mater.* **2016**, 1, 16064.
- [104] A. T. N. Nguyen, J. H. Shim, *RSC Adv.* **2021**, 11, 12520.
- [105] Y. Li, Y. Zhao, H. Cheng, Y. Hu, G. Shi, L. Dai, L. Qu, *J. Am. Chem. Soc.* **2012**, 134, 15.
- [106] R. Atchudan, T. N. J. I. Edison, Y. R. Lee, *J. Colloid Interface Sci.* **2016**, 482, 8.
- [107] L. Qu, Y. Liu, J.-B. Baek, L. Dai, *ACS Nano* **2010**, 4, 1321.
- [108] Y. Shao, S. Zhang, M. H. Engelhard, G. Li, G. Shao, Y. Wang, J. Liu, I. A. Aksay, Y. Lin, *J. Mater. Chem.* **2010**, 20, 7491.
- [109] H. Liu, Q. Zhao, J. Liu, X. Ma, Y. Rao, X. Shao, Z. Li, W. Wu, H. Ning, M. Wu, *Appl. Surf. Sci.* **2017**, 423, 909.
- [110] W.-J. Niu, Y.-P. Wang, J.-Z. He, W.-W. Liu, M.-C. Liu, D. Shan, L. Lee, Y.-L. Chueh, *Nano Energy* **2019**, 63, 103788.
- [111] Y. Liu, R. Ge, Y. Chen, M. Huang, R. Zhu, W. Li, Y. Liu, L. Feng, R. Che, *Chem. Eng. J.* **2021**, 420, 127598.
- [112] X. Gu, Z. Chen, Y. Li, J. Wu, X. Wang, H. Huang, Y. Liu, B. Dong, M. Shao, Z. Kang, *ACS Appl. Mater. Interfaces* **2021**, 13, 24814.
- [113] Y. Xue, B. Huang, Y. Yi, Y. Guo, Z. Zuo, Y. Li, Z. Jia, H. Liu, Y. Li, *Nat. Commun.* **2018**, 9, 1460.
- [114] T. Song, X. Zhang, P. Yang, *Langmuir* **2021**, 37, 4236.
- [115] T. Feng, Q. Zeng, S. Lu, M. Yang, S. Tao, Y. Chen, Y. Zhao, B. Yang, *ACS Sustain. Chem. Eng.* **2019**, 7, 7047.
- [116] T. Feng, G. Yu, S. Tao, S. Zhu, R. Ku, R. Zhang, Q. Zeng, M. Yang, Y. Chen, W. Chen, W. Chen, B. Yang, *J. Mater. Chem. A* **2020**, 8, 9638.

- [117] X. Zhao, H. Liu, Y. Rao, X. Li, J. Wang, G. Xia, M. Wu, *ACS Sustain. Chem. Eng.* **2019**, *7*, 2610.
- [118] Z. Liu, B. Li, Y. Feng, D. Jia, C. Li, Q. Sun, Y. Zhou, *Small* **2021**, *17*, 2102496.
- [119] J. Jana, J. S. Chung, S. H. Hur, *J. Alloys Compd.* **2021**, *859*, 157895.
- [120] Y. Liu, N. Ye, X. Li, X. Li, H. Liu, E. Wang, C. Liang, X. Peng, *J. Solid State Chem.* **2021**, *293*, 121781.
- [121] Y. Ali, V.-T. Nguyen, N.-A. Nguyen, S. Shin, H.-S. Choi, *Int. J. Hydrogen Energy* **2019**, *44*, 8214.
- [122] Q. Dang, Y. Sun, X. Wang, W. Zhu, Y. Chen, F. Liao, H. Huang, M. Shao, *Appl. Catal. B: Environ.* **2019**, *257*, 117905.
- [123] a) L. Liao, H. Peng, Z. Liu, *J. Am. Chem. Soc.* **2014**, *136*, 12194; b) X. Huang, Z. Yin, S. Wu, X. Qi, Q. He, Q. Zhang, Q. Yan, F. Boey, H. Zhang, *Small* **2011**, *7*, 1876.
- [124] S. Biswas, I. Arief, S. S. Panja, S. Bose, *ACS Appl. Mater. Interfaces* **2017**, *9*, 3030.
- [125] a) I. Arief, S. Biswas, S. Bose, *Nano-Struct. Nano-Objects* **2017**, *11*, 94; b) M. Cao, C. Han, X. Wang, M. Zhang, Y. Zhang, J. Shu, H. Yang, X. Fang, J. Yuan, *J. Mater. Chem. C* **2018**, *6*, 4586.
- [126] A. K. Singh, A. N. Yadav, A. Srivastava, K. K. Haldar, M. Tomar, A. V. Alaferdov, S. A. Moshkalev, V. Gupta, K. Singh, *Nanotechnology* **2019**, *30*, 505704.
- [127] a) Y.-Q. Zou, N. von Wolff, A. Anaby, Y. Xie, D. Milstein, *Nat. Catal.* **2019**, *2*, 415; b) H. Song, S. Luo, H. Huang, B. Deng, J. Ye, *ACS Energy Lett.* **2022**, 1043.
- [128] D. N. Nguyen, G. S. Gund, M. G. Jung, S. H. Roh, J. Park, J. K. Kim, H. S. Park, *ACS Nano* **2020**, *14*, 17615.



Samarjeet Singh Siwal is currently working as an assistant professor in Department of Chemistry, MM(DU), Mullana-India. He received his Ph.D. in chemistry from the University of Johannesburg, South Africa, in 2017. Then, he moved to Kunming University of Science and Technology (KUST), China, as a postdoctoral research fellow (under Professor Qibo Zhang). His current research interests include the synthesis and application of 2D materials in different fields such as overall water splitting, supercapacitors, fuel cells, and biosensors. He has published over 55 SCI journal articles, 2 patents, and 03 book chapters.



Harjot Kaur is currently carrying out doctoral degree (under Dr. Samarjeet Singh Siwal and Professor Vijay Kumar Thakur) at Department of Chemistry, Maharishi Markandeshwar (Deemed to be University) Mullana, Ambala, India. She received her bachelor's degree in 2017 from Kurukshetra University, Kurukshetra, India. She did her master's degree in chemistry from Maharishi Markandeshwar (Deemed to be University), Mullana-Ambala, India, in 2020. Her research interests focus on the development of nanocomposites and nanotechnologies for enhanced biosensing and renewable energy technologies.



Adesh K Saini, professor and head of Research & Development, Maharishi Markandeshwar (Deemed to be University), Mullana (HR) India. He gained his Ph.D. in biomedical sciences (University of Delhi/CSIR-IGIB, India). He was a postdoctoral fellow at NICHD-NIH, Bethesda USA. He was ex-dean of Faculty of Sciences and ex-director of Center of Research on Himalayan Sustainability at Shoolini University, Solan India. His research group focuses on redox biology, nano-based antimicrobials, and anticancer therapy and gene regulation. He has published more than 50 patents and over 100 SCI journal articles in the area of microbiology, water purification, and cancer.



Vijay Kumar Thakur is a professor and founding head of the Biorefining and Advanced Materials Research Centre at SRUC, Edinburgh, UK. Before commencing his tenure at SRUC, he has previously held faculty positions at Cranfield University, Washington State University, USA, and Nanyang Technological University, Singapore. His research activities span the disciplines of biorefining, chemistry, manufacturing, materials science, nanotechnology, and sustainable and advanced materials. He has published over 350 SCI journal articles, 2 patents, 52 books, and 40 book chapters. He sits on the editorial board of several SCI journals as an editor/editorial advisory board member.